NASA
Technical
Paper
2061

November 1982

Universal Approach to Analysis of Cavitation and Liquid-Impingement Erosion Data

P. Veerabhadra Rao
and Stanley G. Young

NASA

NASA
Technical
Paper
2061

1982

Universal Approach to Analysis of Cavitation and Liquid-Impingement Erosion Data

P. Veerabhadra Rao
and Stanley G. Young
Lewis Research Center
Cleveland, Ohio

NASA
National Aeronautics
and Space Administration

**Scientific and Technical
Information Branch**

SUMMARY

Most earlier models for the prediction of cavitation and liquid-impingement erosion of materials suffer certain deficiencies and do not precisely predict the magnitude of erosion, particularly during long exposures. Data for several materials tested in both a rotating-disk device and a magnetostriction oscillator have now been analyzed in a different manner that presents normalized cumulative average erosion rate versus normalized time. A universal curve-fitting approach is proposed to attempt to define the complex erosion process. With knowledge of four parameters it may be possible to more closely correlate erosion data between the laboratory model and field device prototypes. These parameters are the maximum erosion rate on the cumulative average erosion rate versus time curve, the time to attain this peak, the incubation period, and the erosion resistance (a measure of the relative strength of the material coupled with the severity of erosion attack). Data analyzed from two previous investigations with entirely different experimental conditions (cavitation and liquid impingement) agreed with the present formulation. This agreement, which showed strong similarities between cavitation and liquid-impingement erosion in both long-term experimental results and model predictions, clearly reinforced the possibility of the universal nature of erosion. Correction factors for the incubation period and material properties (especially for the softer materials) are included to improve the prediction capabilitites of the model for very long-term erosion.

INTRODUCTION

One of the primary objectives of erosion research has been to model long-term laboratory characterization and erosion resistance to field conditions with more confidence and reliability. Honegger (ref. 1) in 1927 was the first investigator to consider "specific erosion" in an attempt to compare materials and time effects. However, more detailed studies pertaining to time effects on erosion rates were not considered until the mid-1960's (refs. 2 to 5). In view of the strong dependence of the erosion rate on exposure time in both cavitation and liquid-impingement environments, several formulations and statistical models were advanced by different investigators (refs. 4 to 11). These studies have been used to quantify the nonlinear effects of the erosion rate versus time curves and to predict accurately the long-term erosion behavior of materials. The main purposes of these formulations were

(1) To identify the damage as well as the erosion mechanisms involved during the erosion process with time
(2) To characterize and predict, as precisely as possible, the erosion rate as the exposure time increases
(3) To test materials in the laboratory for relatively short times and extrapolate these data to materials in the field

Several devices have been used by different investigators to characterize and evaluate a wide spectrum of materials at various laboratory conditions with a variety of liquids (refs. 5 to 18). Valid comparisons of test results, including screening and ranking of different materials, have always been difficult because of the variations in the damage curves and a lack of understanding of the basic mechanisms involved in the resistance of materials, time effects, velocity and size scaling, modeling relations, etc. In view of all these problems, it was generally agreed by many investigators that test results should be compared only if based on the corresponding stages of the erosion rate versus time curves. Specifically, these have been named the in-

cubation period, the acceleration period (accumulation zone), the peak damage rate, the deceleration period (attenuation zone), the steady-state region, and the long-term erosion period, which is characterized as cyclic, decreasing, or increasing depending on the test method and the erosion resistance of the material. Typical rate-time curves reproduced in figure 1 depict all periods (refs. 2 to 5).

A historical background of work on long-time cavitation erosion prediction and the methods for modeling the erosion rate curves are presented in the appendix. No single model or prediction attempt has yet been fully precise in its ability to predict erosion rates during either the initial or advanced stages of erosion. Also the influence of the incubation period (when it exists) on the inception and rate of erosion is not fully understood. Correction or scaling factors used to convert the erosion resistance observed in the laboratory to that observed in prototype devices have not been fully satisfactory. Hence, long-term predictions that used earlier formulations were different from actual data by factors of two or more.

Rather than attempting to increase or decrease the number of variables for prediction purposes, it is essential to consider the accuracy of the prediction and its statistical deviation. Hence, a very simple formulation or a well-defined single curve is all that is required. Ideally, this would enable design engineers to predict the behavior of a material from laboratory testing even before prototype operation. Most prolonged operations of field devices require more confidence-level information if machinery is to operate at optimum efficiency. Thus if an accurate method is devised to predict the long-term erosion of a baseline material and it is found that the erosion thus obtained would be detrimental during the desired performance period, either the material can be changed at the design stage or more accurate overhaul periods can be established.

In this report a method for erosion-rate-data curve fitting is presented as normalized average erosion rate versus normalized time. This method greatly reduces individual variations of the instantaneous erosion rate versus time curves. In this manner, a universal approach to the analysis of data from previous investigations is presented for prediction purposes. The long-term exposure behavior is discussed, and correction factors pertaining to the incubation period and erosion resistance are described.

SYMBOLS

$(MER)_a$	maximum cumulative average erosion rate
$(MER)_i$	maximum instantaneous erosion rate
p	pressure
t	exposure time to cavitation or impingement erosion
$t_a, t_b, t_c, .., t_n$	incubation periods of curves A,B,C...,N in fig. 22
t_{inc}	incubation period of a typical erosion rate versus time curve
t_m	time to attain maximum or peak rate of erosion on a typical erosion rate versus time curve

$t_{m,a}$	time to attain maximum on cumulative average erosion rate versus time curve
$t_{m,i}$	time to attain maximum on instantaneous erosion rate versus time curve
Δt	incremental time causing an incremental volume loss ΔV
V	velocity
V	cumulative volume loss due to cavitation erosion corresponding to t hours exposure
$\mathbf{V}_m$	maximum cumulative volume loss due to cavitation erosion corresponding to t_m hours exposure, or cumulative erosion corresponding to slope of erosion-time curve joining origin and point of tangency
$\Delta \mathbf{V}$	incremental volume loss of material in incremental time Δt

DATA ANALYSIS AND PROCEDURES

Data Sources

In the development of this new curve-fitting approach for long-term cavitation and liquid-impingement erosion rate prediction, data obtained independently over a long time span by each of the present authors was used. One author used a rotating-disk device (refs. 19 and 20) and the other a magnetostriction apparatus (refs. 21 to 23). The original data sets reported earlier were used for the present analysis. The details of the rotating-disk device are presented in figure 2 and described fully in reference 24, and the details of the magnetostriction apparatus are presented in figures 3(a) and (b) for vibrating and stationary specimens, respectively, and described fully in references 21 to 23.

The experimental conditions for the rotating-disk device were as follows: velocity, 35 to 37.3 m/s; pressure, 111 to 170 kPa abs; diameter of the cavitation inducer, 25.4 mm; and test liquid, water. The materials tested were aluminum, copper, brass I, brass II, stainless steel, and mild steel. The compositions of the materials and their properties are presented in tables I and II, respectively. The experimental conditions pertaining to the magnetostriction apparatus were as follows: frequency, 25 kHz; amplitude, 44 μm; test liquids, sodium (from 204° to 649° C) and water. The materials tested were nickel, aluminum, zinc, iron, L-605 cobalt-base alloy, Stellite, and stainless steel. The compositions of the materials and their mechanical properties are presented in tables III and IV, respectively.

Data Treatment Method

Figure 4 presents cumulative erosion versus exposure time curves for stainless steel tested in a rotating-disk device at four different velocities (ref. 19). Figure 5 presents instantaneous erosion rate versus time curves for the same material. The method used for calculating instantaneous erosion rate as local tangents is shown on the upper curve in figure 4. As erosion

resistance increases the incubation period becomes pronounced. Because there are several peaks and valleys in the erosion rate versus time curves, the prediction of erosion rate with exposure time, especially for long times, becomes very difficult.

As a first step to improve the situation, the cumulative average erosion rate was calculated for the same data presented in figure 4 and was plotted versus time in figure 6. The method used for calculating cumulative average erosion rate is shown schematically on the upper curve (V = 37.3 m/s) in figure 4. The oscillations observed in figure 5 are considerably smoothed in figure 6 by this treatment. It is now evident that a material behaves in a similar manner at different velocities and that each erosion rate curve has a maximum if the test has been run for a sufficient length of time. Next, each data point of figures 5 and 6 was normalized with respect to peak erosion rate and the time corresponding to this peak. This was done by calculating the ratios of each data point to the peak rate and the time of each point to the time of the peak rate. Figures 7 and 8 present normalized instantaneous erosion rate versus normalized time and normalized cumulative average erosion rate versus normalized time, respectively. The scatter in figure 7 is too great to provide an accurate model or predictive equation for the field engineer. Any theory or model proposed by earlier investigators does not fit these plots without many assumptions and large scatter bands. On the other hand, figure 8 provides a smooth curve without oscillations, indicating that a material follows a certain natural trend even under different experimental conditions.

RESULTS AND DISCUSSION

Figures 9 and 10 present normalized instantaneous and cumulative average erosion rates versus normalized time for brass II and brass I tested in a rotating-disk device at different velocities. Figures 11 to 14 present the same types of plots for aluminum and mild steel tested in a rotating-disk device at different pressures. Figures 15 to 17 show the same parameters for different materials tested as vibrating and stationary specimens in a magnetostriction apparatus.

The peaks of the instantaneous and cumulative average erosion rates, the times to attain them, and their ratios for the materials tested in a rotating-disk device and a magnetostriction apparatus are presented in tables V and VI, respectively. From observations of parts (a) of figures 9 to 17, which present normalized instantaneous erosion rate versus normalized time, it is apparent that there is much scatter and that most of the individual materials cannot be represented by any single formulation. On the other hand, parts (b) of figures 9 to 17, which show normalized cumulative average erosion rate versus normalized time for the same materials, show a dramatic reduction in scatter from the corresponding parts (a). This again indicates that a consistent pattern exists for the curves when cumulative average erosion rate is used instead of instantaneous erosion rate. This consistent configuration was observed not only for materials tested in a rotating-disk device using water, but also for a variety of materials tested in a magnetostriction apparatus using water as well as liquid sodium.

The ratio of instantaneous to cumulative peak heights varied from 1.0 to 3.87 for different materials tested in the rotating-disk device and from 1.0 to 1.71 for different materials tested with the magnetostriction apparatus using water and liquid sodium (tables V and VI). As would be expected, the times to attain maximum cumulative average erosion rate $t_{m,a}$ were always

longer than the times to attain maximum instantaneous erosion rate $t_{m,i}$. It is further clear from tables V and VI that for different materials tested the ratio $t_{m,i}/t_{m,a}$ varied from 0.42 to 0.96 in the rotating-disk device and from 0.30 to 0.88 in the magnetostriction apparatus. As the erosion resistance of the material increased, the ratio $(MER)_i/(MER)_a$ decreased. There was no clear-cut trend for the ratio $t_{m,i}/t_{m,a}$.

The advantages of normalized cumulative average erosion rate versus normalized time plots are (1) that scatter of the instantaneous erosion rate-time curves is partly reduced and results in a consistent, relatively smooth set of curves; and (2) that the $(MER)_a$ and $t_{m,a}$ can be evaluated from fewer experimental points on the erosion-time curve.

Comparisons with Earlier Investigations

Before proceeding with a generalized plot to represent long-term, cavitation and liquid-impingement erosion processes for all types of materials, data reported by Kerr (ref. 25) and Thomas and Brunton (ref. 26) were analyzed in the same manner as in the present investigations and are presented in figures 18 and 19. The improvement in cumulative average erosion rate (figs. 18(b) and 19(b)) is clear. This data treatment further supports the view that the normalized cumulative average erosion rate versus time curves have significant advantages for erosion prediction with reduced data scatter. It was noted from figures 8, 9(b), and 19(b) and the quantitative data in tables V and VI that brass II and stainless steel tested at different experimental conditions agreed very well on the normalized average basis. Hence, it may be inferred that, irrespective of the type of device used to produce erosion, qualitative and quantitative correlations exist between cavitation and liquid impingement.

Effect of Time Increments on Prediction Models

There is always a question as to how many experimental points are necessary and what time intervals should be used in order to arrive at predictions that are as precise as possible. To investigate the effect of the length of exposure intervals on the accuracy of the final plots, figures 20(a) and (b) were plotted using 1-hour intervals for cavitation data of the alloy L-605 in liquid sodium at 427° C. The same curves with close intervals are presented in figures 15(a) and(b), respectively. Major differences can be noted by comparing the two sets of data.

If there are fewer points, the determination of maximum erosion rate and t_m will be affected as shown in table VII. Parameters calculated at 60-min intervals are far less accurate than those calculated at 5-, 10-, and 15-min intervals. Errors of 50 to 300 percent were observed in determining the parameters $(MER)_a$ and $t_{m,a}$. As the erosion resistance decreased, the error increased for long-interval experiments (table VII). Figures 15 and 20 indicate, however, that close-interval data need be collected only until an accurate peak is attained. After that it may not be necessary to obtain many additional points at close intervals. Since $(MER)_a$ and $t_{m,a}$ are the crucial parameters that are used to calculate the requisite quantities, errors involved in their determination will lead to much greater inaccuracies when they are used for long-term predictions. This study clearly points out the importance of using close intervals in the early stages of erosion (up to the peak rate of erosion) to arrive at precise parameters for prediction purposes.

Effect of Very Long Exposures on Erosion Rates

Ever since investigators have been aware of the influence of test time on the erosion rate there has been controversy regarding the long-term erosion rate. Some investigators have reported continuous decreases after the initial peak rate, some have reported constant final rates (steady state), and others report cyclic rates at even longer exposures. All of these patterns have been well documented (refs. 2 to 6, 12, 27 to 35). Cumulative average erosion rate versus time curves presented in figure 21 in the normalized form generally show a decreasing trend irrespective of erosion resistance and material (refs. 19 and 22).

The very long-term exposure plots presented in this figure are unique as the ratio $t/t_{m,a}$ was obtained up to nearly 400 (the highest ratio believed to be observed to date). Some of the deviations from a smooth curve in these plots are believed to be due to the small number of data points taken during the incubation and acceleration periods. As explained in the previous section, difficulties in obtaining the true values of $(MER)_a$ and $t_{m,a}$ were partially responsible for the difficulty in obtaining a universal plot.

Incubation Period Correction

In this section the influence of the incubation period is discussed and a correction factor is presented to account for its use. A typical set of most commonly observed average erosion rate versus time curves are schematically represented in figure 22(a). The incubation periods are indicated in the figure as t_a, t_b, and t_c (and designated in general as t_{inc}). By subtracting these times from the time of each experimental point on each of the respective curves t_m, a condensed set of plots was generated (fig. 22(b)). The new normalized time for peak erosion rate is now calculated as $(t - t_{inc})/(t_m - t_{inc})$.

All plots of normalized cumulative average erosion rate and normalized time use the relationships $(\mathbf{V}/t)/(\mathbf{V}_m/t_m)$ and t/t_m, respectively. A correction factor for incubation period as used in figure 22(b) is necessary for all the previous figures, and this would cause them to shift toward the y axis by the amount of time equivalent to the incubation period. In making the transition from model to prototype the incubation period for the prototype relative to the model should be known in order to make this correction for more accurate long-term predictions.

Recently Heymann (ref. 36), while analyzing the ASTM G-2 sponsored "round robin" test program, found that comparisons and correlations using the average peak erosion rate gave more scatter and inconsistency than those using the instantaneous peak erosion rate. This is primarily due to the dependence of the incubation period on average erosion rate, and there is more scatter in incubation periods than in maximum erosion rates (ref. 36). A possible disadvantage of the incubation period correction suggested here is that it may sometimes remove one of the major attractions of the original average erosion rate approach. Therefore it is not used in the final analysis forwarded in this paper.

Erosion Resistance Variation

Laboratory and field devices produce uneven erosion over the test speci-

men; hence, calculations for erosion resistance are very general and would vary considerably even within the same device or test.

The normalized average cumulative erosion rate versus time curves in the present investigations, though generally smooth, indicate some deviations with erosion intensity. It was generally observed that as the erosion resistance decreased, the portions of the curves following the peaks attained a lower value at long test times. For a single test device these portions of the curves for more resistant materials were lower at long times. The height of each curve at longer test times appears to be a function of both the device and the material. This observation of a correlation between the level of the long-term erosion rate versus time curve and erosion resistance may be helpful in applying this universal plot approach to data from both laboratory and field devices.

Universal Approach Plots

Summary plots of normalized average erosion rate versus normalized time are presented in figures 23(a) to (c) using the experimental data for brass, stainless steel, and mild steel, respectively, from all the previous figures. Every material tested in any type of cavitation or liquid-impingement device can be represented in this manner. Depending on the test device and material tested, a mean curve can be chosen and scatter bands can be defined or derived. The accuracy of the derivation of the two parameters $t_{m,a}$ and $(MER)_a$ (including the incubation period) contributes to the accuracy of the prediction. The deviation is greater in the normalized time region from 0 to 1 than it is in any other portion of the curve. Greater deviations can be expected if incubation corrections are not considered.

Although the plots of figure 23 are similar to the set of plots reported by another investigator (ref. 6), figure 23 is based on experimental data without any assumptions or direct relation to theory. The plots of reference 6 were generated by using instantaneous erosion rate versus time; the curves of figure 23 were developed by using cumulative average erosion rate versus time. Equations proposed in reference 8, which use both tangent points and fixed average depth of erosion values combined with a curve-fitting approach, result in much wider variations than those reported herein.

The concept of normalized cumulative average erosion rate versus normalized time was used by Heymann (ref. 8) and by one of the present authors (refs. 19 and 20) to check the validity of the erosion theory proposed in reference 6 for a rotating-disk device. It was found that using cumulative average erosion rate instead of instantaneous erosion rate considerably reduced the scatter and the plots were closer to the theoretical curves presented in reference 6. The use of cumulative average erosion rate was also considered in references 8 and 33. Normalized instantaneous erosion rate versus normalized time curves have also been presented for erosion-corrosion modeling using a magnetostriction apparatus (ref. 34) and for steam turbine blade and shield materials using four different impingement devices (ref. 35). The investigator of reference 33 also suggested that only two parameters $(MER)_a$ and $t_{m,a}$ can be used to predict average erosion rates for materials. However, the current report shows the importance of the incubation period and the erosion resistance in prediction attempts.

The erosion process due to cavitation and liquid impingement is believed to be a function of the earlier history of the eroded surface (including work hardening, surface stresses, and changes in material properties). Also, a

study of the relationship between the surface roughness and the erosion rate would be helpful to gain additional insight into the erosion process at longer times.

SUMMARY OF RESULTS

Data for a large number of materials tested in both a rotating-disk device and a magnetostriction apparatus were analyzed in a new manner that brought the results of the two methods closer to a universal curve fit.

Normalized cumulative average erosion rate was plotted versus normalized time, and a curve fit was proposed that covers a comprehensive variety of materials, test conditions, and devices. Cumulative average erosion rate and time were normalized to the peak damage rate and the time to peak damage rate, respectively. Adjustments were suggested for incubation periods.

It was shown that the universal approach plot is more accurate if small time increments are used before the peak damage rate is reached. After the peak damage rate is passed, at long exposure times, more resistant materials show a lower normalized average erosion rate.

The curves and data scatter bands derived from this universal curve-fitting approach appear to be useful in correlating different types of laboratory tests with each other and with field data.

Lewis Research Center
National Aeronautics and Space Administration
Cleveland, Ohio, May 7, 1982

APPENDIX - AN OVERVIEW OF LONG-TERM CAVITATION EROSION PREDICTIONS AND MODELING METHODS

Prediction equations or models to estimate erosion rates as a function of time have been formulated by Heymann (refs. 4 and 8), Thiruvengadam (ref. 6), Hoff and Langbein (ref. 7), Tichler and de Gee (ref. 5), Engel (ref. 9), Perelman and Denisov (ref. 10), Noskievic (ref. 11), and others (refs. 12 to 17). The important models and formulations and the variables necessary to evaluate the erosion rate versus time for each of them are presented in table VIII. However, a brief description of each contribution along with the assumptions is given here in order to explain the current status of erosion rate - time predictions and models.

Heymann (ref. 4) developed a statistical model to predict erosion rate - time patterns under impingement and cavitation erosion conditions for different materials where fatigue is the predominant failure mechanism. The assumptions in the formulation are (1) that each small surface element is subjected to an impact fatigue environment and after a certain time (i.e., a certain number of impacts) it will be detached from the surface as an erosion fragment because of subsurface fatigue failure and (2) that considering many such surface elements the time required for their removal is described by a statistical distribution function similar to that for the number of cycles to failure of a large number of conventional fatigue specimens. In the preliminary model Heymann used normal distribution truncated and normalized over a finite time span. On the other hand, in his more complex model he adopted the log-normal distribution function. This model permits specification of a different distribution function for each level below the original surface and two different functions for the original surface. The model requires input of four parameters to obtain instantaneous erosion rate versus time curves similar to many of those observed in real situations.

An erosion theory proposed by Thiruvengadam (ref. 6) is based on the concepts of accumulation and attenuation of impact energy using a fatigue probability function. The final equation quantitatively predicts the relative intensity of erosion with relative time. The basic assumptions of the theory are (1) that the attenuation of the bubble collapse energy is inversely proportional to the n^{th} power of the radial distance and (2) that the intensity of erosion is related to the intensity of impact with a material property (erosion strength) governing the efficiency of energy absorption, which is always time dependent. The final equation also requires input of four parameters to compute a curve of normalized instantaneous erosion rate versus normalized time.

An exponential function incorporating the heterogeneous impingement characteristics of impacting drops based on impact statistics was obtained for the rate of erosion by Hoff and Langbein (ref. 7). The proposed equation is as follows:

$$I_{hl} = 1 - e^{-t_i/t} \tag{1}$$

where

I_{hl} relative erosion rate with respect to peak rate of erosion

t_i incubation period (intercept on time axis extended from linear portion of erosion-time curve)

t exposure time

The assumptions involved are similar to other statistical models. However, it should be noted that when a Poisson distribution is introduced into the method proposed by Heymann (ref. 4) or a distribution function is introduced into the method proposed by Hoff and Langbein (ref. 7), the two methods are quite similar. With the equation proposed by Hoff and Langbein only two parameters are required to compute the erosion rate as a function of time.

Heymann (ref. 8) in 1969 suggested a simple curve-fitting approach to estimating the erosion rate that follows the peak erosion rate. This curve used an exponential equation of the form

$$I_h = Ae^{-BY_h} \tag{2}$$

(which seems to have some influence on the formula originally suggested by Hoff and Langbein in 1964 (ref. 7)). Here I_h is the normalized erosion rate with respect to tangent erosion rates at each point, Y_h is the normalized mean depth of erosion with respect to tangent mean depth of erosion at each point, and B is a constant. This equation needs three parameters to compute erosion rate versus time curves on a normalized scale. Heymann (ref. 8) also modified equation (2) to estimate the time required to reach a particular mean depth of erosion on the surface of a material by using the erosion rate and velocity as well as the erosion rate and hardness relationships.

Tichler and de Gee (ref. 5) have derived a formula for the mean depth of erosion versus time relationship in the attenuation and final steady-state periods in mathematical and physical terms.

The assumptions for the equation are as follows:

(1) The rate of erosion does not keep attenuating because the surface cannot contain more than a certain number of craters per unit area. (This results in a second steady-state period.)

(2) The difference between the rate of erosion during the first steady-state period and that in the attenuation period is proportional to the number of craters per unit area.

(3) The rate of crater formation is proportional to the number of craters that can still be formed (the difference between the number of craters per unit area in the final steady-state period and at any time).

This equation needs five parameters to define the erosion rate versus time curve.

Using the concepts developed by Thiruvengadam (refs. 6 and 13 to 15), Kohl (ref. 12) developed several scaling laws to model cavitation damage with respect to time. The analyses were checked by data obtained from a vibratory cavitation device and a rotating-foil apparatus.

Using surface strength statistics, Engel (ref. 9) and Perelman and Denisov (ref. 10) advanced different analytical formulations. Engel's model had numerous valid and generous assumptions; whereas Perelman and Denisov's analysis was similar to the statistical model proposed by Heymann (ref. 4). Using his erosion strength theory (ref. 16), Thiruvengadam generated a nomogram that was based on cavitation erosion data. With this device the life of a particular material can be estimated as a function of erosion intensity; or conversely, with a knowledge of the operation period and intensity of erosion (erosion strength), the depth of erosion can be calculated. Using extensive data sets from the literature, Springer (ref. 17) developed a model on fatigue concepts and on the assumptions that the incubation period, the acceleration period,

and the maximum rate of erosion of a characteristic erosion curve can be represented by a linear relationship. Rao, et al. (ref. 18) presented an empirical relationship to predict the time required to pierce a hole through specimens in a rotating-disk device by cavitation, using the incubation period of the same material at the identical hydrodynamic conditions. Neither Springer nor Rao considered long-term erosion rate predictions.

Recently, Noskievic (ref. 11) formulated a mathematical relaxation model for the dynamics of cavitation attack that uses a differential equation applied to forced oscillations with damping. The primary assumptions used in this model are as follows:

(1) The coefficients for internal friction and the measure of cavitation strength of materials are constant during plastic deformation.

(2) The intensity of cavitation attack (indicated as the power consumption per unit area) is also constant.

This cavitation erosion model requires three parameters for prediction efforts.

REFERENCES

1. Honegger, E.: Tests on Erosion Caused by Jets. Brown Boveri Rev., vol. 14, no. 4, Apr. 1927, pp. 96-104.

2. Thiruvengadam, A.; and Preiser, H. S.: On Testing Materials for Cavitation Damage Resistance. Journal of Ship Research, vol. 8, no. 3, Dec. 1964, pp. 39-56.

3. Plesset, M. S.; and Devine, R. E.: Effect of Exposure Time on Cavitation Damage. J. Basic Eng., vol. 68, no. 4, Dec. 1966, pp. 691-705.

4. Heymann, F. J.: On Time Dependence of Rate of Erosion Due to Impingement or Cavitation. Am. Soc. Test. Mater. Spec. Tech. Publ. (408), 1967, pp. 70-110.

5. Tichler, J. W.; and de Gee, A. W. J.: Time Dependence of Cavitation Erosion and Effect of Some Material Properties. Proc. Third Intern. Conf. on Rain Erosion and Associate Phenomena, Vol. II, A. A. Fyall and R. B. King, eds., Royal Aircraft Establishment, Farnborough, England, 1970, pp. 847-879.

6. Thiruvengadam, A.: Theory of Erosion. Proc. Second Meersburg Conf. on Rain Erosion and Allied Phenomena, Vol. II, A. A. Fyall and R. B. King, eds., Royal Aircraft Establishment, Farnborough, England, 1967, pp. 605-653.

7. Hoff, G; and Langbein, G.: Resistance of Materials Towards Various Types of Mechanical Stress. Proc. Second Meersburg Conf. on Rain Erosion and Allied Phenomena, Vol. II, A. A. Fyall and R. B. King, eds., Royal Aircraft Establishment, Farnborough, England, 1967, pp. 655-681.

8. Heymann, F. J.: Toward Quantitative Prediction of Liquid Impact Erosion. Am. Soc. Test. Mater. Spec. Tech. Publ. (474), 1970, pp. 212-248.

9. Engel, O. G.: A First Approach to a Microscopic Model of Erosion Rate in Drop Impact and Cavitation. Proc. Third Intern. Conf. on Rain Erosion and Associate Phenomena, Royal Aircraft Establishment, Farnborough, England, Aug. 1970, pp. 447-518.

10. Perelman, R. G.; and Denisov, Y. D.: Strength of Materials Under the Action of Droplet Impacts. Royal Aircraft Establishment Library Translation No. 1654, 1971 (Primary Source - Probl. Prochn., vol. 10, 1971, pp. 20-26 (In Russian.))

11. Noskievic, J.: Dynamics of the Cavitation Damage. Proc. Joint IAHR-ASME-ASCE Symposium on Design and Operation of Fluid Machinery, Vol. II, Colorado State University, 1978, pp. 453-462.

12. Kohl, R. E.: Experimental Studies to Establish Scaling Laws for Modeling Cavitation Damage Intensity. Tech. Report 233-12, Hydronautics, Inc., June 1968. (AD-675939.)

13. Thiruvengadam, A.: The Concept of Erosion Strength. Am. Soc. Test. Mater. Spec. Tech. Publ. (408), 1967, pp. 22-41.

14. Thiruvengadam, A.: On The Selection of Modeling Materials to Scale Long Term Erosion Behavior of Prototype Systems. Proc. Third Intern. Conf. on Rain Erosion and Allied Phenomena, Royal Aircraft Establishment, Farnborough, England, Aug. 1970.

15. Thiruvengadam, A.: Scaling Laws for Cavitation Erosion. Tech. Report 233-15, Hydronautics, Inc., Dec. 1971. (AD-736934.)

16. Schmitt, G. F., Jr.: Liquid and Solid Particle Impact Erosion. Wear Control Handbook, M. B. Peterson and W. O. Winer, eds., ASME, 1981, pp. 231-282.

17. Springer, G. S.: Erosion by Liquid Impact. Scripta Publishing Co., John Wiley & Sons, 1976.

18. Rao, P. V.; et al.: Estimation of Cavitation Erosion with Incubation Periods and Material Properties. J. Test. Eval., vol. 9, no. 3, May 1981, pp. 189-197.

19. Rao, P. V.: Characteristics, Correlations, Similarities and Prediction of Erosion due to Cavitation and Liquid Impingement. Ph.D. Thesis, Indian Institute of Science, Bangalore, India, Sept. 1975.

20. Rao, N. S. L.; Rao, P. V.; and Rao, B. C. S.: A Study of Cavitation Erosion in Rotating Components. Proc. Fifth Conf. on Fluid Machinery, vol. 1, Budapest, Hungary, 1975, pp. 603-613.

21. Young, S. G.: Cavitation Damage of Stainless Steel, Nickel, and Aluminum Alloy in Water for ASTM Round Robin Tests. NASA TM X-1670, 1968.

22. Young, S. G.; and Johnston, J. R.: Effect of Temperature and Pressure on Cavitation Damage in Sodium. Am. Soc. Test. Mater. Spec. Tech. Publ. (474), 1970, pp. 67-108.

23. Young, S. G.: Study of Cavitation Damage to High Purity Metals and a Nickel-Base Superalloy in Water. NASA TN D-6014, 1970.

24. Rao, P. V.; Rao, B. C. S.; and Rao, N. S. L.: Erosion and Cavity Characteristics in Rotating Components. J. Test. Eval., vol. 8, no. 3, May 1980, pp. 127-142.

25. Kerr, S. L.: Determination of the Relative Resistance to Cavitation Erosion by the Vibratory Method. Trans. ASME, vol. 59, no. 5, July 1937, pp. 373-397.

26. Thomas, G. P.; and Brunton, J. H.: Drop Impingement Erosion of Metals. Proc. R. Soc. London, ser. A, vol. 314, no. 1519, Jan. 1970, pp. 549-565.

27. Young, S. G.; and Johnston, J. R.: Accelerated Cavitation Damage of Steels and Superalloys in Sodium and Mercury. Am. Soc. Test. Mater. Spec. Tech. Publ. (408), 1967, pp. 186-212.

28. Hirotsu, M.: Cavitation Damage Mechanism and Its Correlation to Physical Properties of Material. Am. Soc. Test. Mater. Spec. Tech. Publ. (474), 1970, pp. 48-66.

29. Thiruvengadam, A.; Rudy, S. L.; and Gunasekaran, M.: Experimental and Analytical Investigations on Liquid Impact Erosion. Am. Soc. Test. Mater. Spec. Tech. Publ. (474), 1970, pp. 249–287.

30. Matsumura, M.: Influence of Test Parameters in Vibratory Cavitation Erosion Tests. Am. Soc. Test. Mater. Spec. Tech. Publ. (664), 1979, pp. 434–458.

31. Rao, P. V.; and Rao, B. C. S.: Some Erosion Studies and Scale Effects with Rotating Disk Device. Cavitation Erosion in Fluid Systems, W. L. Swift and R. E. A. Aandt, eds., ASME, 1981, pp. 119–131.

32. Heymann, F. J.: Progress and Problems in Erosion Prediction - From a Design Engineering Point of View. Engineering Report E-1503. Westinghouse Electric Corp., Feb. 1974.

33. Lichtarowicz, A.: Cavitating Jet Apparatus for Cavitation Erosion Testing Erosion. Am. Soc. Test. Mater. Spec. Tech. Publ. (664), 1979, pp. 530–549.

34. McGuinness, T.; and Thiruvengadam, A.: Cavitation Erosion - Corrosion Modeling. Am. Soc. Test. Mater. Spec. Tech. Publ. (567), 1974, pp. 30–55.

35. Elliott, D. E.; Marriott, J. B.; and Smith, A.: Comparison of Erosion Resistance of Standard Steam Turbine Blade and Shield Materials on Four Test Rigs. Am. Soc. Test. Mater. Spec. Tech. Publ. (474), 1970, pp. 127–161.

36. Heymann, F. J.: Conclusion from the ASTM Interlaboratory Test Program with Liquid Impact Erosion Facilities. Proc. 5th Intern. Conf. on Erosion by Solid and Liquid Impact, Cambridge, England, 1979, paper 20.

37. Murphy, A. J.: Nonferrous Foundry Metallurgy. Pergamon Press (London), 1954.

38. Lyman, T.: Metals Handbook. Vol. I. American Society for Metals, 1961.

39. Wear Resistant Alloys. Bulletin No. F30-1-33-A, Haynes Stellite Co., 1962.

40. Weiss, V.; Sessler, J. G., eds.: Aerospace Structural Metals Handbook. 3rd revision. AMS Specifications L605-AMS5759B, Syracuse University Press, 1966.

TABLE I. - NOMINAL COMPOSITION OF MATERIALS TESTED

Component	Material		
	Brass I[a]	Mild steel[b]	Stainless steel[b]
	Composition, wt %		
Copper	95.1	--	--
Aluminum	.4	--	--
Iron	1.0	99.1	62.0
Manganese	2.5	.5	2.5
Tin	.5	--	--
Nickel	.5	--	14.0
Carbon	--	.3	.08
Silicon	--	.05	1.0
Chromium	--	--	18.0
Molybdenum	--	--	2.5
Phosphorus	--	.1	--

[a]Ref. 37.
[b]Ref. 38.

TABLE II. - MECHANICAL AND OTHER PROPERTIES OF MATERIALS[a]

Property	Material					
	Aluminum	Copper	Brass I	Brass II	Mild steel	Stainless steel
Density, kg/m^3	2.70×10^3	8.95×10^3	8.50×10^3	8.50×10^3	7.85×10^3	7.80×10^3
Yield strength, MPa	63.3	97.7	108.2	104.9	334.3	244.5
Tensile strength, MPa	83.4	180.5	213.9	202.1	448.8	637.7
Elastic modulus, GPa	69.0	117.2	110.4	110.4	193.2	193.2
Brinell hardness, H scale	28	58	150	141	95	170
Elongation, percent	7	43	46	41	6	57
Reduction in area, percent	28	48	52	45	47	55
Strain energy,[b] MN-m/m^3	7.2	65.8	81.8	75.4	22.6	254.4
Ultimate resilience,[c] N-m/m^3	5.0×10^4	13.9×10^4	20.7×10^4	18.5×10^4	52.1×10^4	105.3×10^4
Modified resilience[d]	0.17	0.44	1.43	1.27	1.08	2.75
Fracture strength, MPa	69.7	115.8	158.4	184.2	380.2	542.5

[a]Modified resilience and ultimate resilience are included as single properties because they have the dimensions of single properties even though different individual properties are involved in them.
[b]Area under the engineering stress-strain curve of the material.
[c]Ultimate resilience = (Tensile strength)^2/2 x Elastic modulus.
[d]Modified resilience = (Tensile strength x Hardness)/2 x Elastic modulus. The units are generally expressed in terms of hardness units.

TABLE III. - NOMINAL CHEMICAL COMPOSITIONS OF TEST MATERIAL

Component	Material							
	Stellite 6B[a]	L-605 AMS 5759B[b]	AISI 316 stainless steel AMS 5648C[b]	Zinc	Ni-270[c]	Ni-270[d]	Iron	6061-T6 aluminum[d]
	Composition, wt %							
Iron	[e]3	[e]3	Balance	0.0015	0.001	---	99.842	[e]0.7
Nickel	[e]3	10	13	--	99.981	99.98	--	--
Cobalt	Balance	Balance	--	--	.001	--	--	--
Chromium	30	20	18	--	.001	--	--	.25
Molybdenum	[e]1.5	--	2.5	--	--	--	--	--
Tungsten	4.5	15	--	--	--	--	--	--
Carbon	1.1	.1	.08	--	.01	.005	.025	--
Manganese	[e]2	1.5	1.6	--	.001	--	.054	.15
Silicon	[e]2	1.0	1.0	--	.001	--	--	.6
Phosphorus	--	.04	.04	--	--	--	.006	--
Sulfur	--	.03	.03	--	.001	--	.011	--
Copper	--	--	.05	--	.001	--	.062	.25
Zinc	--	--	--	99.997	--	--	--	--
Lead	--	--	--	.001	--	--	--	--
Cadmium	--	--	--	.0005	--	--	--	--
Aluminum	--	--	--	--	--	--	--	Balance
Titanium	--	--	--	--	.001	--	--	--
Magnesium	--	--	--	--	.001	--	--	1.0

[a]Ref. 39.
[b]Aerospace materials specifications.
[c]Ref. 23.
[d]Ref. 21.
[e]Maximum.

TABLE IV. - MECHANICAL PROPERTIES OF TEST MATERIALS

Property	Material							
	Stellite 6B[a]	L-605[b]	AISI 316 stainless steel	Zinc[c]	Ni-270[c]	Ni-270[d]	Iron[c]	6061-T6 aluminum[d]
Density, kg/m^3	8.38×10^3	9.13×10^3	7.98×10^3	7.13×10^3	8.90×10^3	8.94×10^3	$7.87 \cdot 10^3$	2.71×10^3
Ultimate yield strength, MPa	9.5×10^2	8.2×10^2	4.8×10^2	1.07×10^2	3.54×10^2	3.36×10^2	2.99×10^2	3.28×10^2
Yield strength, MPa	4.9	2.5	1.9	0.46	0.62	0.55	1.48	2.81
Elongation, percent	29	76	40	9	70	61	52	21.5

[a]Ref. 39.
[b]Ref. 40.
[c]Ref. 23.
[d]Ref. 21.

TABLE V. - MAXIMUM RATE OF EROSION AND TIME TO ATTAIN IT FOR VARIOUS MATERIALS - ROTATING DISK DEVICE

[Investigator, Rao (ref. 19); cavitation inducer diameter, 25.4 mm; water temperature, 32° + 2° C.]

Material	Pressure, kPa abs	Velocity, m/s	Maximum rate of erosion,[a] mm^3/hr		$\frac{(MER)_i}{(MER)_a}$	Time to attain maximum erosion, min		$\frac{t_{m,i}}{t_{m,a}}$[b]
			Instantaneous, $(MER)_i$	Average, $(MER)_a$		Instantaneous, $t_{m,i}$	Average, $t_{m,a}$	
Stainless steel	150	35	0.23	0.08	2.875	68.0	82.5	0.824
		35.3	2.99	.86	3.477	39.5	71.	.556
		36.6	2.92	1.26	2.317	68.	71.	.958
		37.3	5.	2.31	2.165	16.	38.	.421
Brass I	150	35	[c].30	[c].13	2.308	[c]12.	[c]23.	.522
		35.8	[c].51	.19	2.684	[c]19.	23.	.826
		36.6	[c]1.37	.59	2.322	[c]20.	21.	.952
Brass II	150	35	[d].74	.22	3.364	[d]15.	18.	.833
		35.8	[c]1.46	.63	2.317	[c]11.5	14.	.821
		36.6	6.6	3.19	2.069	15.	16.	.938
Aluminum	111	36.6	128.5	107.2	1.199	1.75	3.0	.583
	124	↓	232.5	232.5	1.000	.25	.5	.500
	137		[c]23.2	[c]16.4	1.415	[c] 2.5	[c] 3.0	.833
	150	↓	157	138	1.138	.75	1.0	.750
	111	35.8	52.	26.9	1.933	6.5	8.0	.813
	124	↓	[c]66.2	45.7	1.449	[c] .75	1.5	.500
	137		89.	[d]28.3	3.145	11.0	[d]14.0	.786
	150	↓	[c]78.	78.	1.000	.25	.5	.500
	111	35	[c]20.5	15.1	1.358	[c] 3.5	4.0	.875
	124	↓	37.6	23.1	1.628	1.25	3.0	.417
	137		[c]63.1	39.3	1.606	[c] 1.5	2.0	.750
	150	↓	46.6	46.6	1.000	.25	.5	.500
Mild steel	150	37.3	8.6	4.80	1.792	16.	18.	.889
	163	37.3	[c]3.6	.93	3.871	[c]11.	19.5	.564
	176	37.3	.72	.33	2.182	1.25	1.5	.833

[a]$(MER)_i$ denotes maximum instantaneous erosion rate, mm^3/hr; $(MER)_a$ denotes maximum average erosion rate, mm^3/hr.
[b]$t_{m,i}$ denotes time to attain maximum instantaneous erosion rate, hr; $t_{m,a}$ denotes time to attain maximum average erosion rate, hr.
[c]First peak rate of erosion on instantaneous erosion rate versus time curve.
[d]Second peak rate of erosion on instantaneous erosion rate versus time curve.

TABLE VI. - MAXIMUM RATE OF EROSION AND THE TIME TO ATTAIN IT FOR VARIOUS MATERIALS - MAGNETOSTRICTION APPARATUS

[Amplitude, 44.5 μm; frequency, 25 kHz.]

Investigator	Material	Maximum rate of erosion, mm^3/hr		$\frac{(MER)_i}{(MER)_a}$	Time to attain maximum erosion rate, min		$\frac{t_{m,i}}{t_{m,a}}$	Remarks
		Instantaneous, $(MER)_i$	Average, $(MER)_a$		Instantaneous, $t_{m,i}$	Average, $t_{m,a}$		
Young (ref. 21)	Nickel 270	6.18	5.34	1.157	60	120	0.500	Water at 23.9° C and 10^5 Pa
	6061-T6 aluminum	45.72	38.22	1.196	50	120	.417	
Young (ref. 23)	Nickel	3.24	2.52	1.286	210	240	.875	Water at 23.9° C and 10^5 Pa; distance between specimen and head, 0.51 mm
		2.64	2.10	1.257	105	240	.438	Distance between specimen and head, 0.64 mm
	Zinc 2	232.86	141.54	1.645	42.5	75	.567	Distance between specimen and head, 0.64 mm
	Iron	5.16	2.88	1.792	390	540	.722	Distance between specimen and head, 0.64 mm
	Annealed nickel	4.26	3.30	1.291	165	300	.550	Distance between specimen and head, 0.64 mm
Young and Johnson (ref. 22)	L-605	16.02	12.36	1.296	75	90	.833	Liquid sodium at 204° C and $2x10^5$ Pa
		37.62	28.20	1.334	22.5	30	.750	Liquid sodium at 204° C and $3x10^5$ Pa
		76.20	60.00	1.270	10	15	.667	Liquid sodium at 204° C and $4x10^5$ Pa
		22.80	14.22	1.603	75	120	.625	Liquid sodium at 427° C and $2x10^5$ Pa
		42.78	33.60	1.273	22.5	45	.500	Liquid sodium at 427° C and $3x10^5$ Pa
		85.80	88.20	.923	10	15	.667	Liquid sodium at 427° C and $4x10^5$ Pa
		23.58	14.46	1.631	37.5	90	.417	Liquid sodium at 649° C and $2x10^5$ Pa
		54.00	42.18	1.280	22.5	30	.750	Liquid sodium at 649° C and $3x10^5$ Pa
		58.20	54.78	1.062	10	15	.667	Liquid sodium at 649° C and $4x10^5$ Pa
	Stellite	16.80	9.84	1.707	90	300	.300	Liquid sodium at 427° C and $2.7x10^5$ Pa
		17.10	17.10	1.000	30	60	.500	Liquid sodium at 427° C and $4x10^5$ Pa
	Stainless steel	5.22	4.62	1.130	150	180	.833	Liquid sodium at 427° C and $1x10^5$ Pa
		70.98	70.98	1.000	30	60	.500	Liquid sodium at 427° C and $4x10^5$ Pa

TABLE VII. - MAXIMUM RATE OF EROSION AND TIME TO ATTAIN IT FOR L-605 ALLOY IN A MAGNETOSTRICTION APPARATUS WITH SMALL AND LARGE INTERVALS OF TIME

[Test liquid, liquid sodium at 427° C; amplitude, 44.5 μm; frequency, 25 kHz; specimen, vibrating; data from ref. 22.]

Pressure, Pa	Maximum rate of erosion, mm^3/hr				Time to attain maximum rate of erosion, min			
	Short intervals, 5 and 10 min		Long intervals, 60 min		Short intervals, 5 and 10 min		Long intervals, 60 min	
	Instantaneous, $(MER)_i$	Average, $(MER)_a$	Instantaneous, $(MER)_i$	Average, $(MER)_a$	Instantaneous, $t_{m,i}$	Average, $t_{m,a}$	Instantaneous, $t_{m,i}$	Average, $t_{m,a}$
$2x10^5$	22.80	14.22	16.62	12.96	75	120	90	80
3	42.78	33.60	31.80	31.80	22.5	45	[a]30	[a]60
4	85.80	88.20	46.62	46.62	10	15	[a]30	[a]60

[a]Minimum calculation time possible when calculated by this method.

TABLE VIII. – PREDICTIVE MODELS, FORMULATIONS, AND PARAMETERS NECESSARY FOR COMPUTATION OF CAVITATION AND LIQUID-IMPINGEMENT EROSION CURVES

Investigator	Type of erosion	Year	Parameters needed for computation
Heymann (ref. 4)	Cavitation and liquid impingement (elementary model)	1967	(1) Nominal mean lifetime for original surface (2) Standard deviation for original surface (3) Nominal mean lifetime for substructure (4) Standard deviation for substructure
Heymann (ref. 4)	Liquid impingement (elaborated model)	1967	(1) Delay time during which no failure occurs (2) Mean of log-normal distribution on logarithmic time scale (3) Standard deviation of log-normal distribution on logarithmic time scale
Thiruvengadam (ref. 6)	Liquid impingement and cavitation	1967	(1) Magnitude of instantaneous erosion rate at first peak (2) Time to attain first-peak instantaneous erosion rate (3) Attenuation exponent (4) Weibull shape parameter
Hoff and Langbein (ref. 7)	Liquid impingement (rain erosion)	1967	(1) Maximum rate of erosion (2) Incubation period (intercept on time axis from straight line portion of erosion-time curve
Heymann (ref. 8)	Cavitation and liquid impingement	1971	(1) Mean depth of erosion at tangent point (2) Average erosion rate at tangent point (3) Exponential constant
Heymann (ref. 8)	Liquid impingement	1971	(1) Cumulative mean depth of erosion or material loss at tangent point (2) Normal component of impact velocity (3) Volume of liquid impinging per unit area per unit time (4) Generalized nondimensional erosion resistance parameter
Tichler and de Gee (ref. 5)	Cavitation	1971	(1) Incubation time (2) Resistance against cavitation erosion under hydrodynamic conditions, as occur in magnetostrictive oscillator (3) Mean depth of erosion at which effect of crater formation becomes manifest (4) Proportionality constant, symbolizing increase in mean depth of erosion that would be necessary to form number of craters per unit area in final steady-state period (5) Ratio of rate of erosion in the final steady-state period to rate of erosion in first steady-state period
Noskievic (ref. 11)	Cavitation	1978	(1) Cavitation property of material (2) Cavitation strength of material or inner friction of material during plastic deformation (3) Cavitation damage rate in developed period of cavitation attack
Rao and Young	Cavitation and liquid impingement	Present	(1) Peak cumulative average erosion rate (2) Time to attain peak cumulative average erosion rate (3) Incubation period (4) Erosion resistance

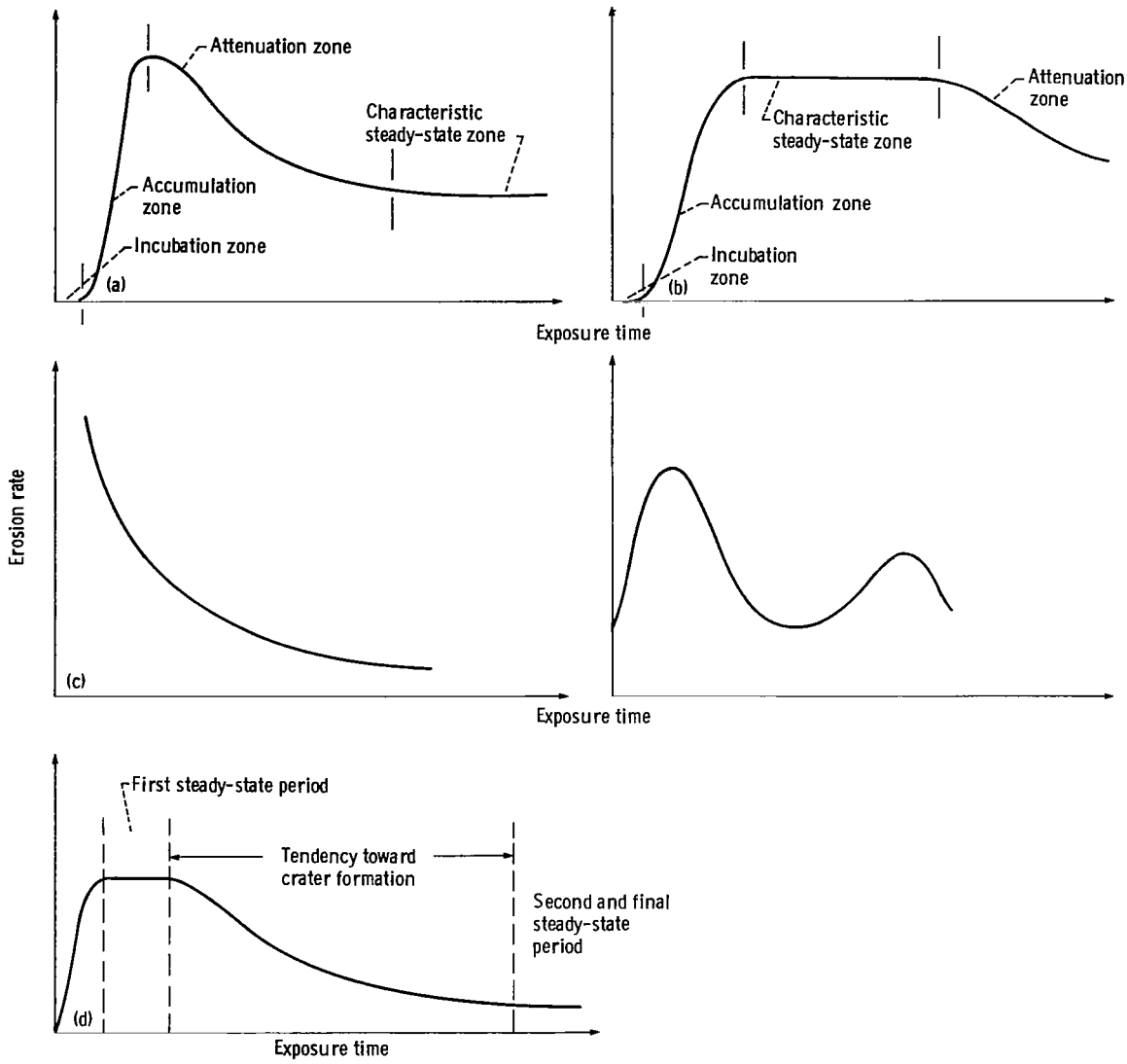

(a) Thiruvengadam and Preiser (ref. 2). (b) Plesset and Devine (ref. 3).
(c) Heymann (ref. 4). (d) Tichler and de Gee (ref. 5).

Figure 1. - Characteristic erosion rate - time curves.

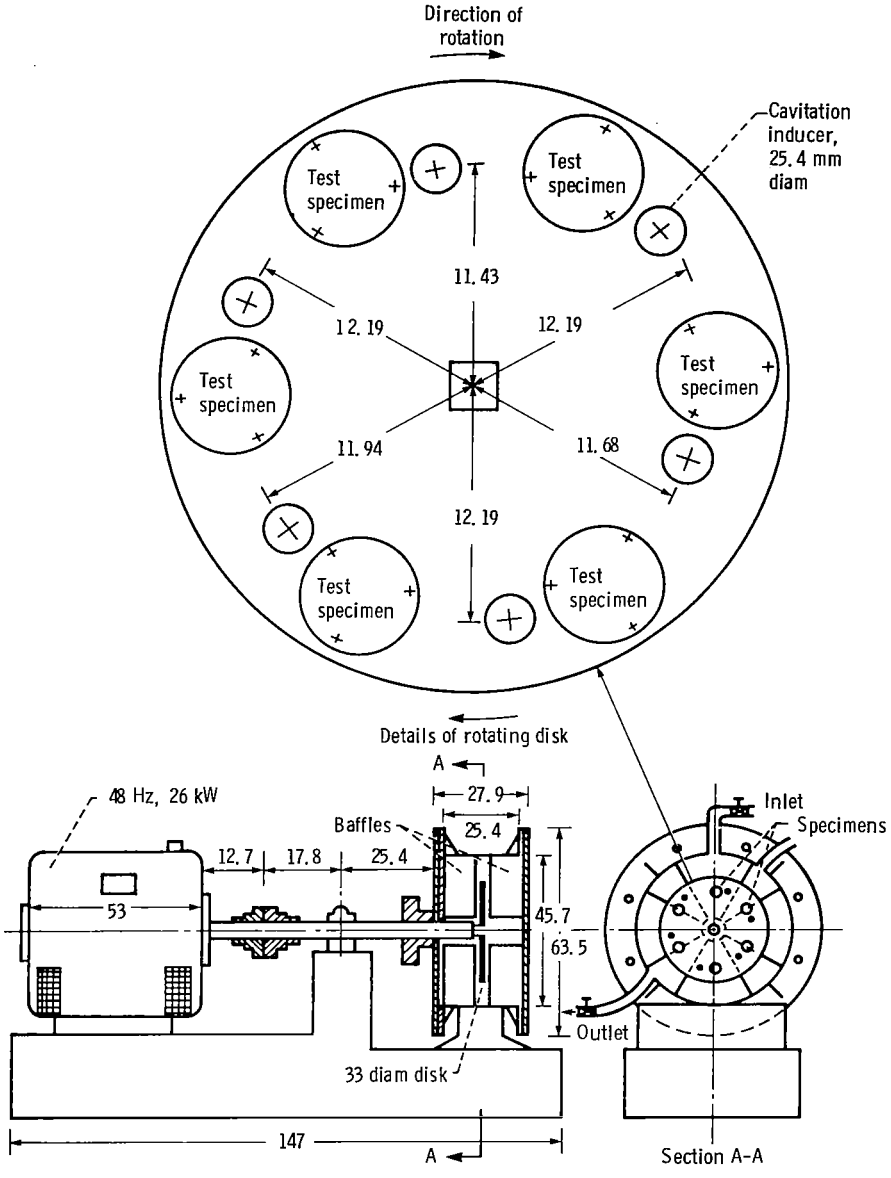

Figure 2. - Sectional views of rotating-disk device. (All dimensions are in centimeters.)

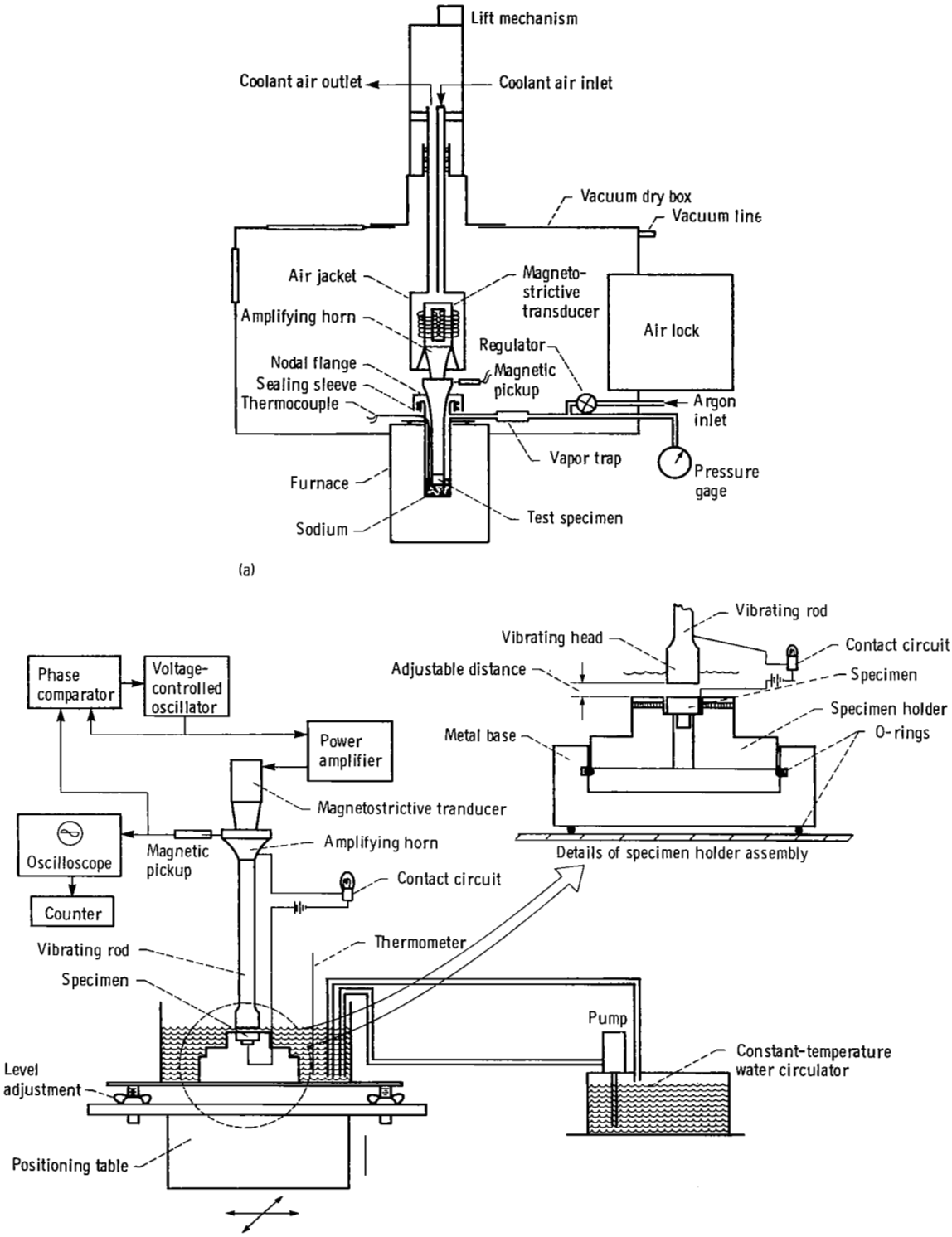

(a) Vibrating test specimen.

(b) Stationary test specimen.

Figure 3. - Schematic diagram of magnetostriction cavitation apparatus.

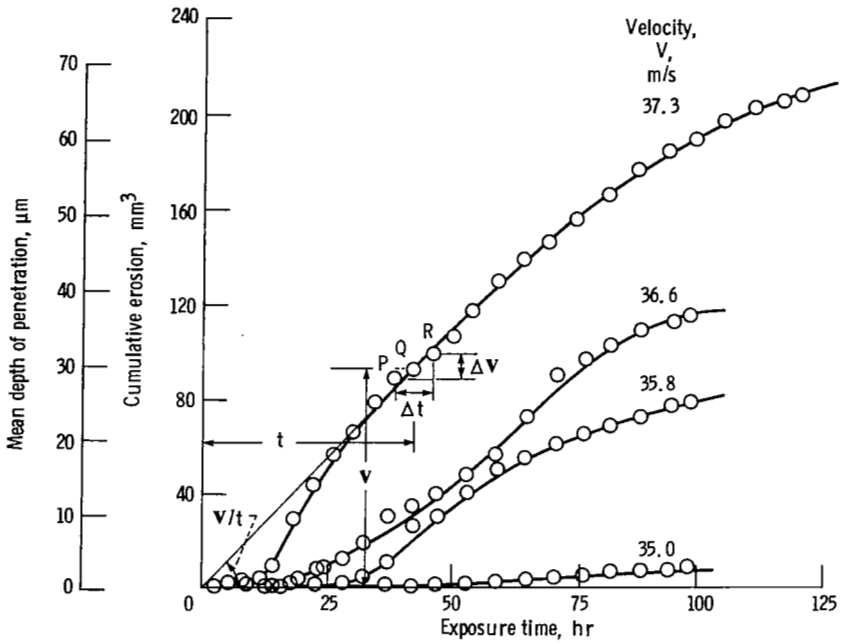

Figure 4. - Cumulative erosion versus time for stainless steel tested in rotating-disk device. Pressure, 150 kPa abs; inducer diameter, 25.4 mm. Instantaneous erosion rate at Q equals slope of local tangent at Q = $\Delta v/\Delta t$; cumulative average erosion rate at Q equals slope of line joining origin and point Q = v/t.

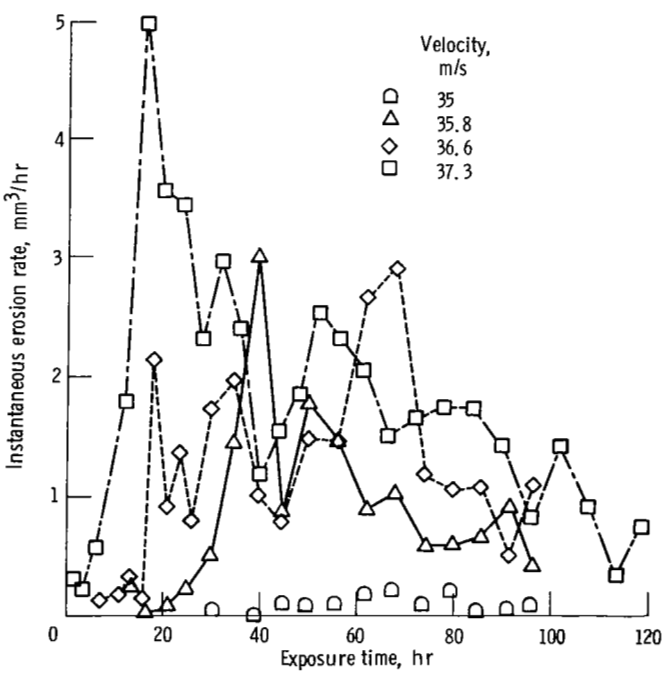

Figure 5. - Instantaneous erosion rate versus time for stainless steel tested in rotating-disk device at various velocities. Pressure, 150 kPa abs.

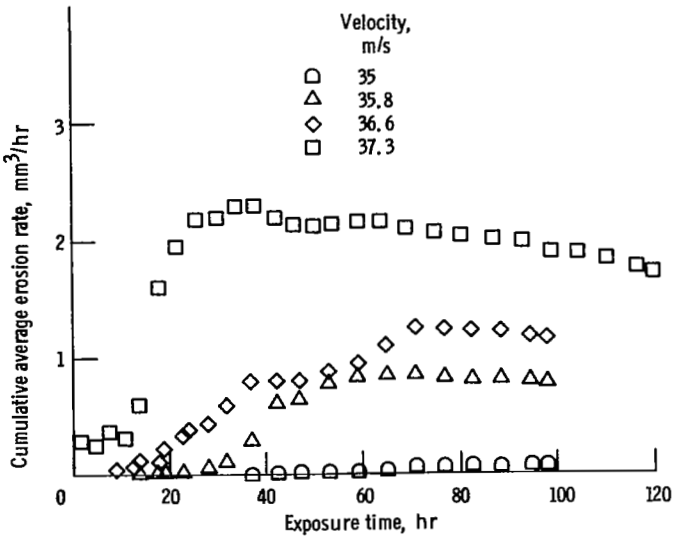

Figure 6. - Cumulative average erosion rate versus time for stainless steel tested in rotating-disk device at various velocities. Pressure, 150 kPa abs.

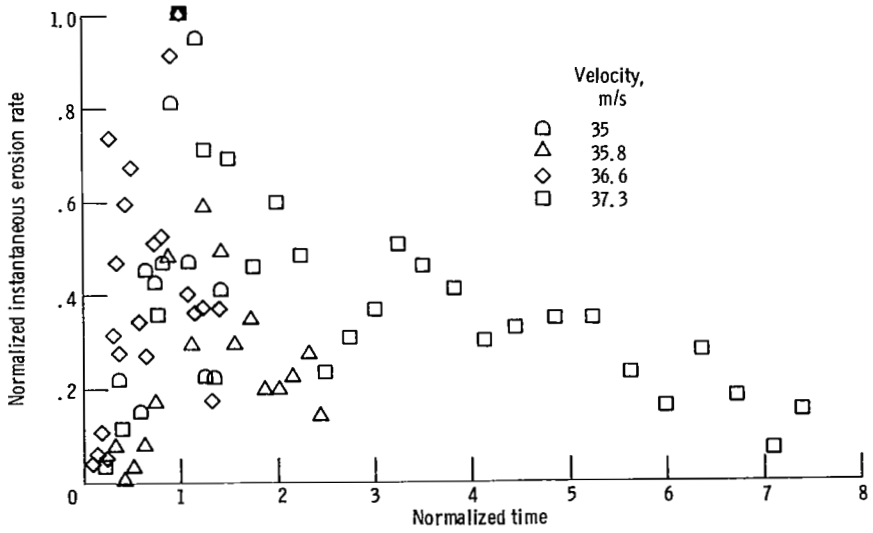

Figure 7. - Normalized instantaneous erosion rate versus normalized time for stainless steel tested in rotating-disk device at various velocities. Pressure, 150 kPa abs.

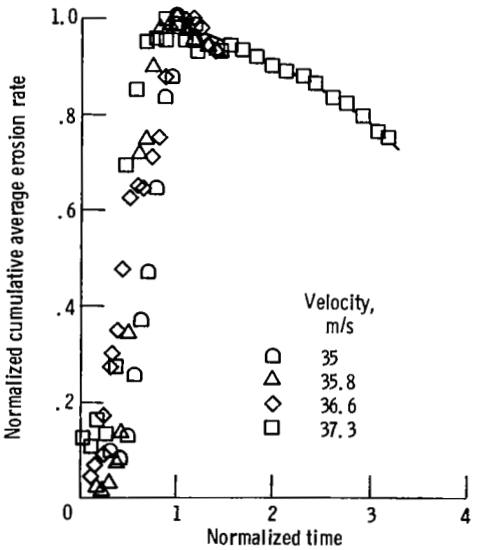

Figure 8. - Normalized cumulative average erosion rate versus normalized time for stainless steel tested in rotating-disk device at various velocities. Pressure, 150 kPa abs.

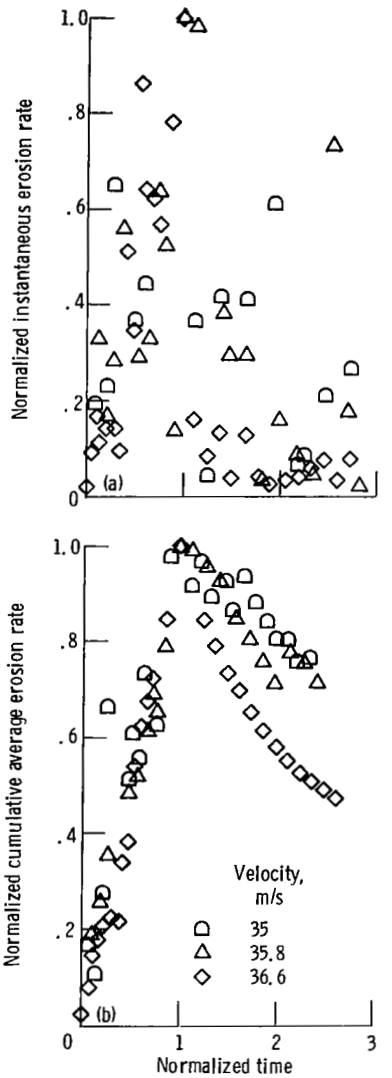

(a) Instantaneous erosion rate.

(b) Cumulative average erosion rate.

Figure 9. - Normalized erosion rate versus normalized time for brass II tested in rotating-disk device at various velocities. Pressure, 150 kPa abs.

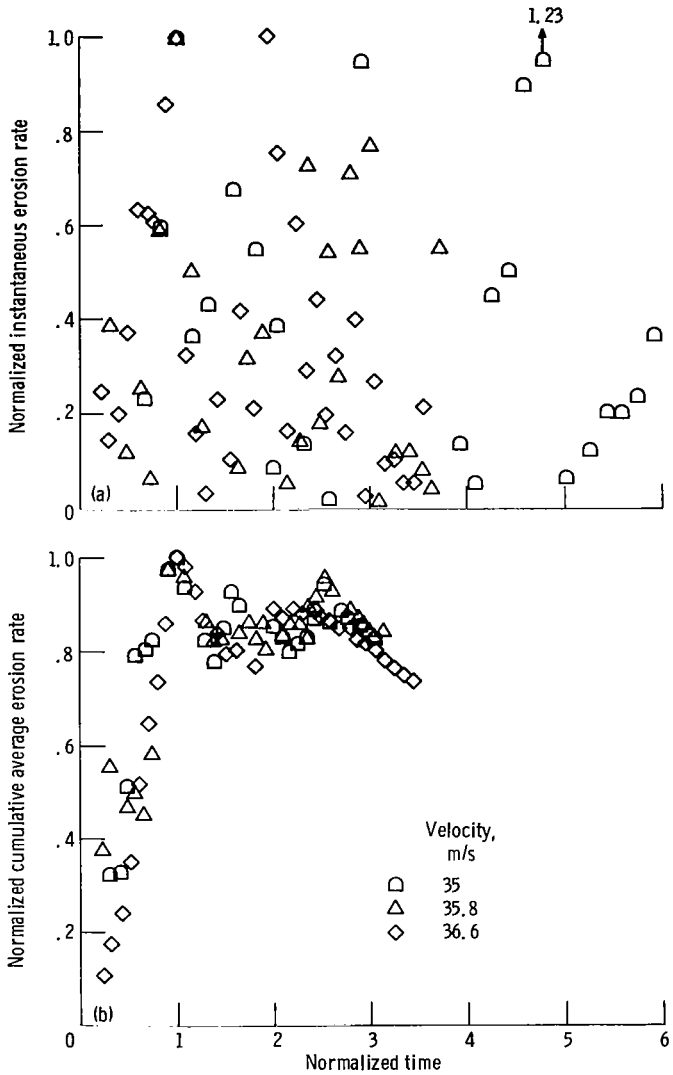

(a) Instantaneous erosion rate.

(b) Cumulative average erosion rate.

Figure 10. - Normalized erosion rate versus normalized time for brass I tested in rotating-disk device at various velocities. Pressure, 150 kPa abs.

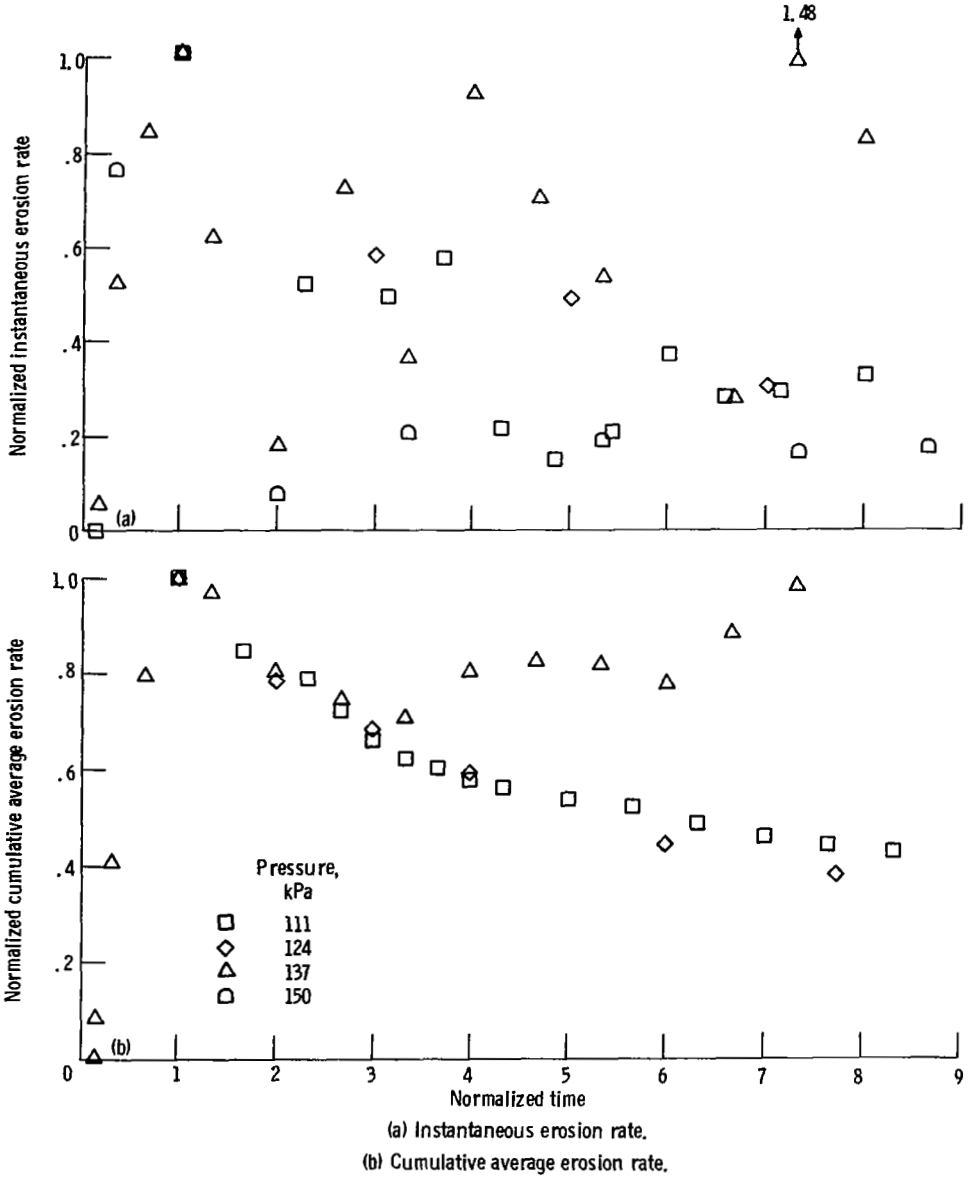

(a) Instantaneous erosion rate.

(b) Cumulative average erosion rate.

Figure 11. - Normalized erosion rate versus normalized time for aluminum tested in rotating-disk device at various pressures - velocity, 36.6 m/s.

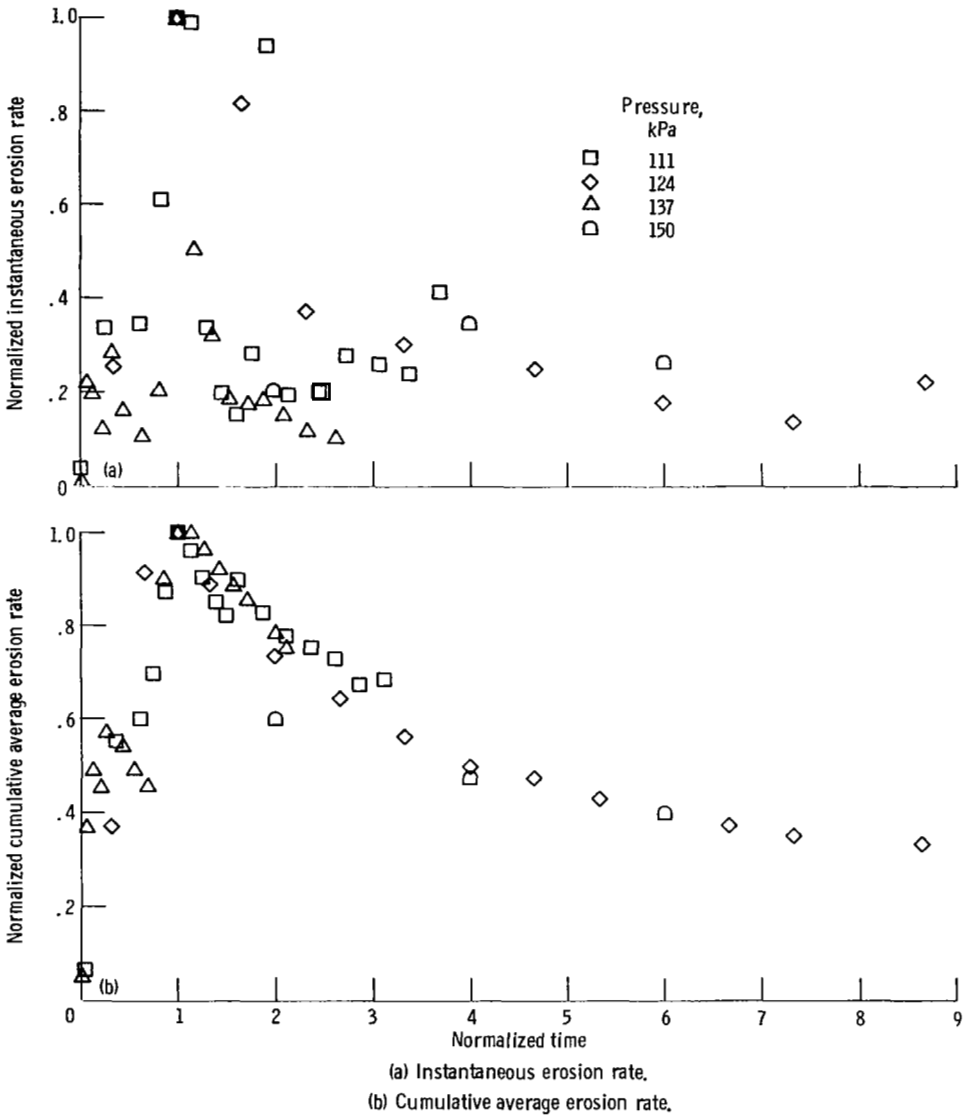

(a) Instantaneous erosion rate.

(b) Cumulative average erosion rate.

Figure 12. - Normalized erosion rate versus normalized time for aluminum tested in rotating-disk device at various pressures - velocity, 35.8 m/s.

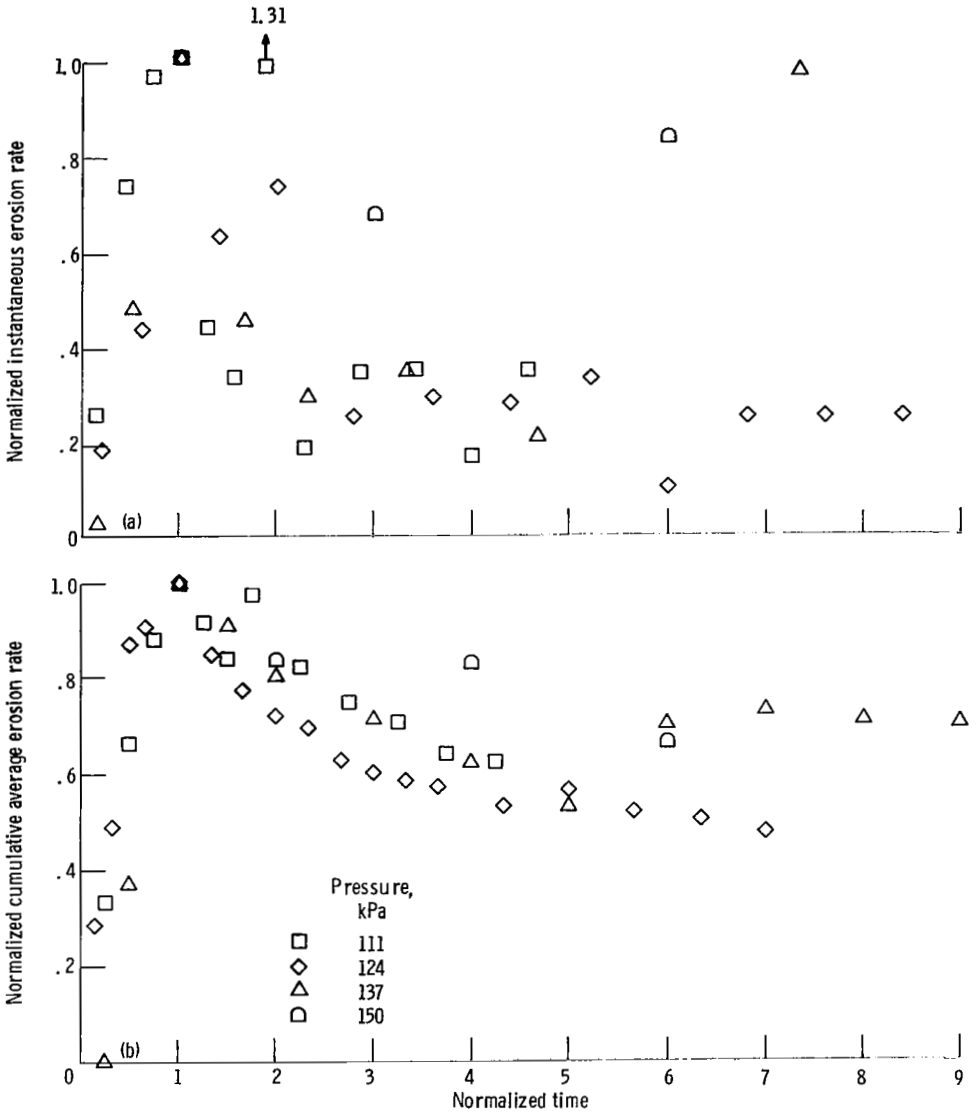

(a) Instantaneous erosion rate.

(b) Cumulative average erosion rate.

Figure 13. - Normalized erosion rate versus normalized time for aluminum tested in rotating-disk device at various pressures - velocity, 35 m/s.

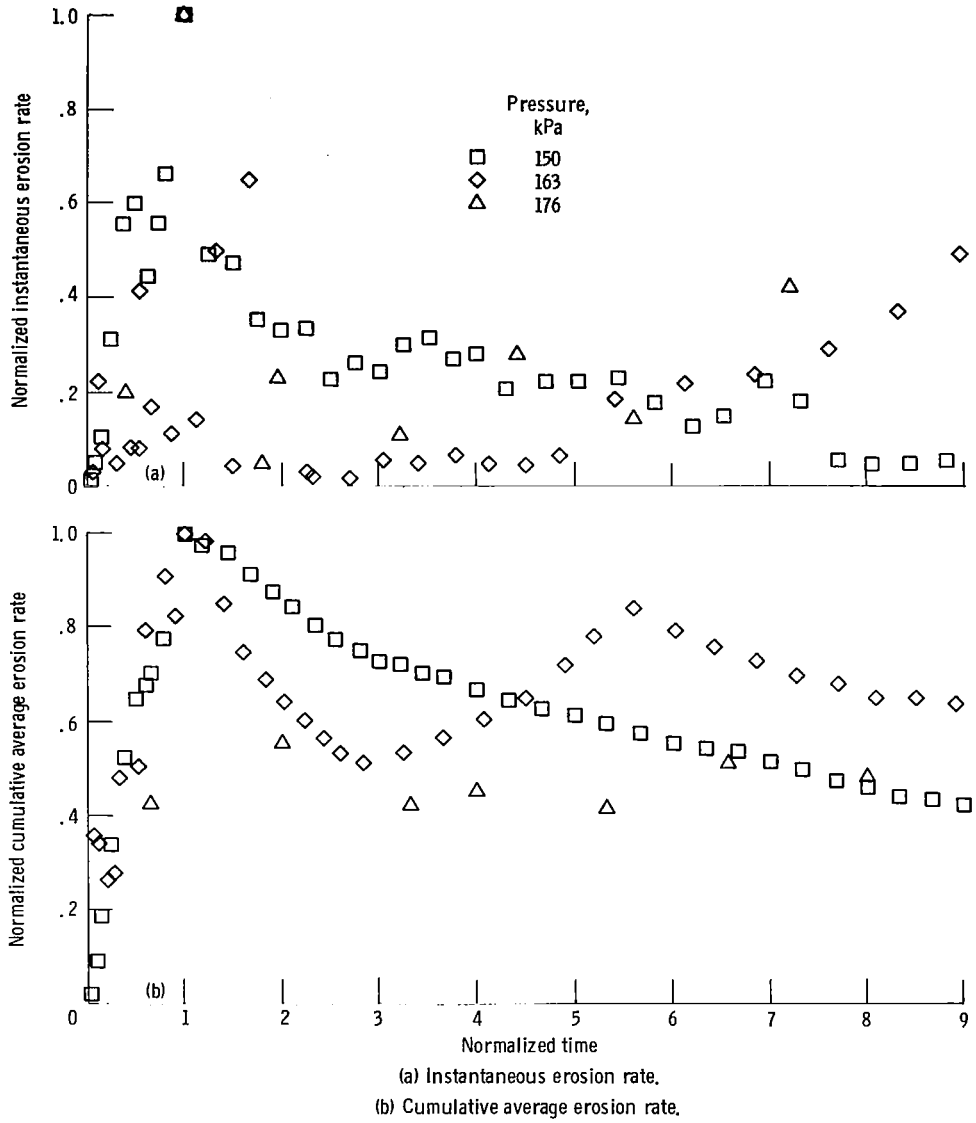

(a) Instantaneous erosion rate.
(b) Cumulative average erosion rate.

Figure 14. - Normalized erosion rate versus normalized time for mild steel tested in rotating-disk device at various pressures - velocity, 37.3 m/s.

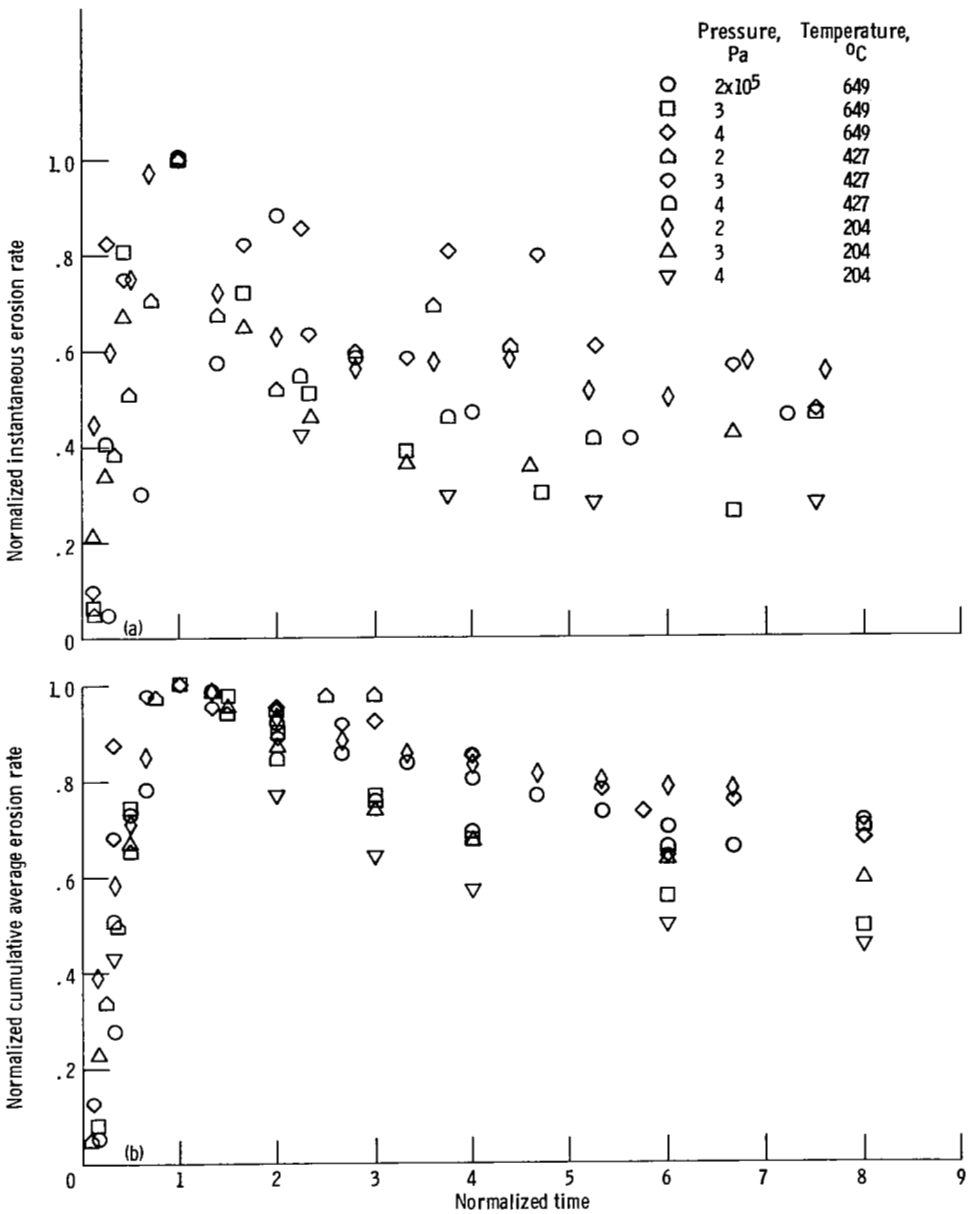

(a) Instantaneous erosion rate.

(b) Cumulative average erosion rate.

Figure 15. - Normalized erosion rate versus normalized time for L-605 alloy tested in magnetostriction apparatus at various temperatures and pressures in liquid sodium.

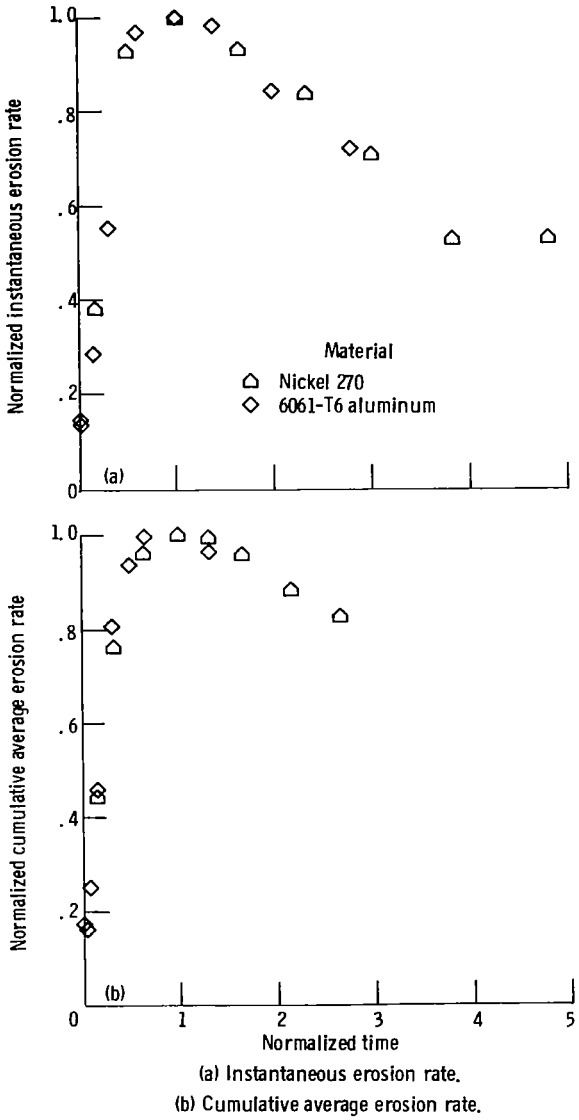

(a) Instantaneous erosion rate.

(b) Cumulative average erosion rate.

Figure 16. - Normalized erosion rate versus normalized time for nickel 270 and 6061-T6 aluminum tested in magnetostriction apparatus in water. Atmospheric pressure; room temperature.

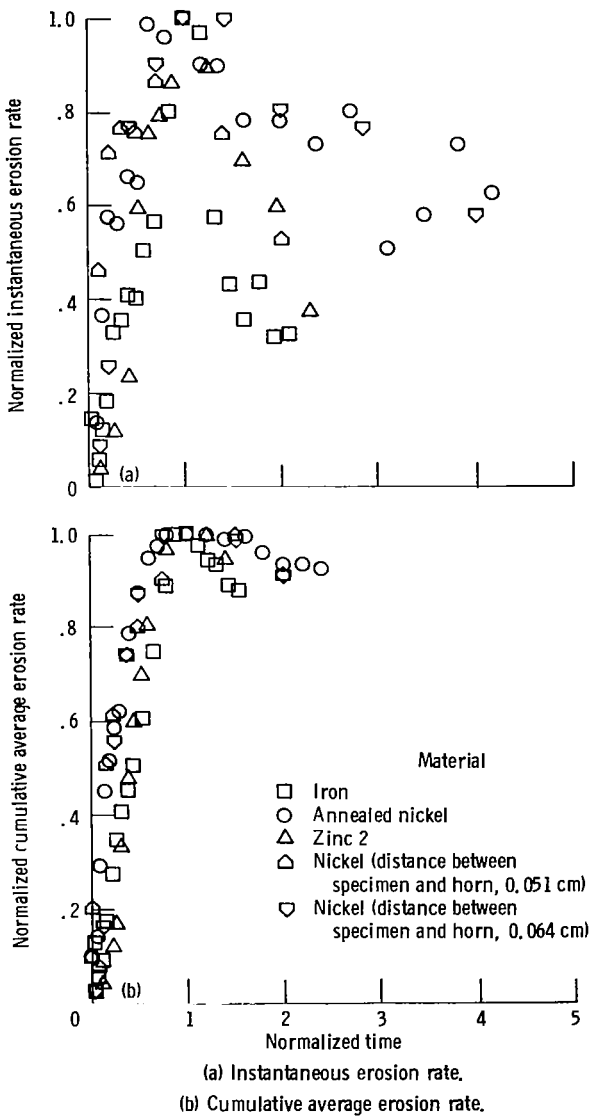

(a) Instantaneous erosion rate.

(b) Cumulative average erosion rate.

Figure 17. - Normalized erosion rate versus normalized time for various materials tested in magnetostriction apparatus in water. Atmospheric pressure; room temperature.

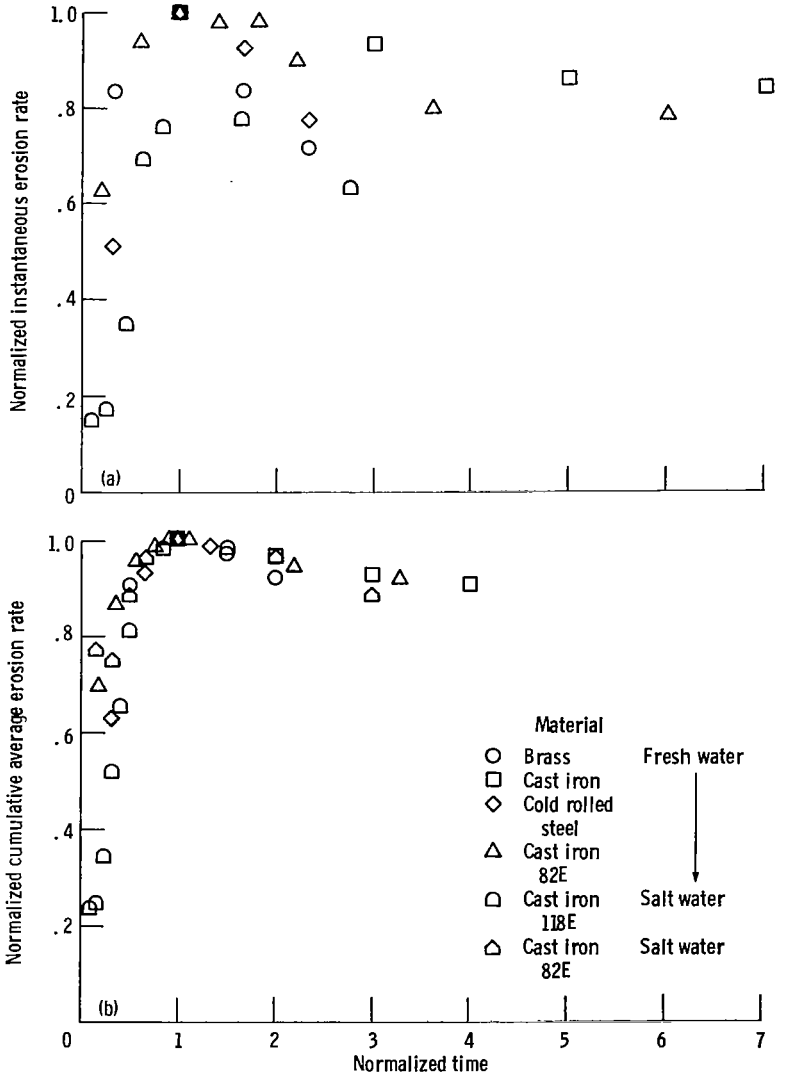

(a) Instantaneous erosion rate.

(b) Cumulative average erosion rate.

Figure 18. - Normalized erosion rate versus normalized time for various materials tested in vibratory cavitation in water. (Data from ref. 25.)

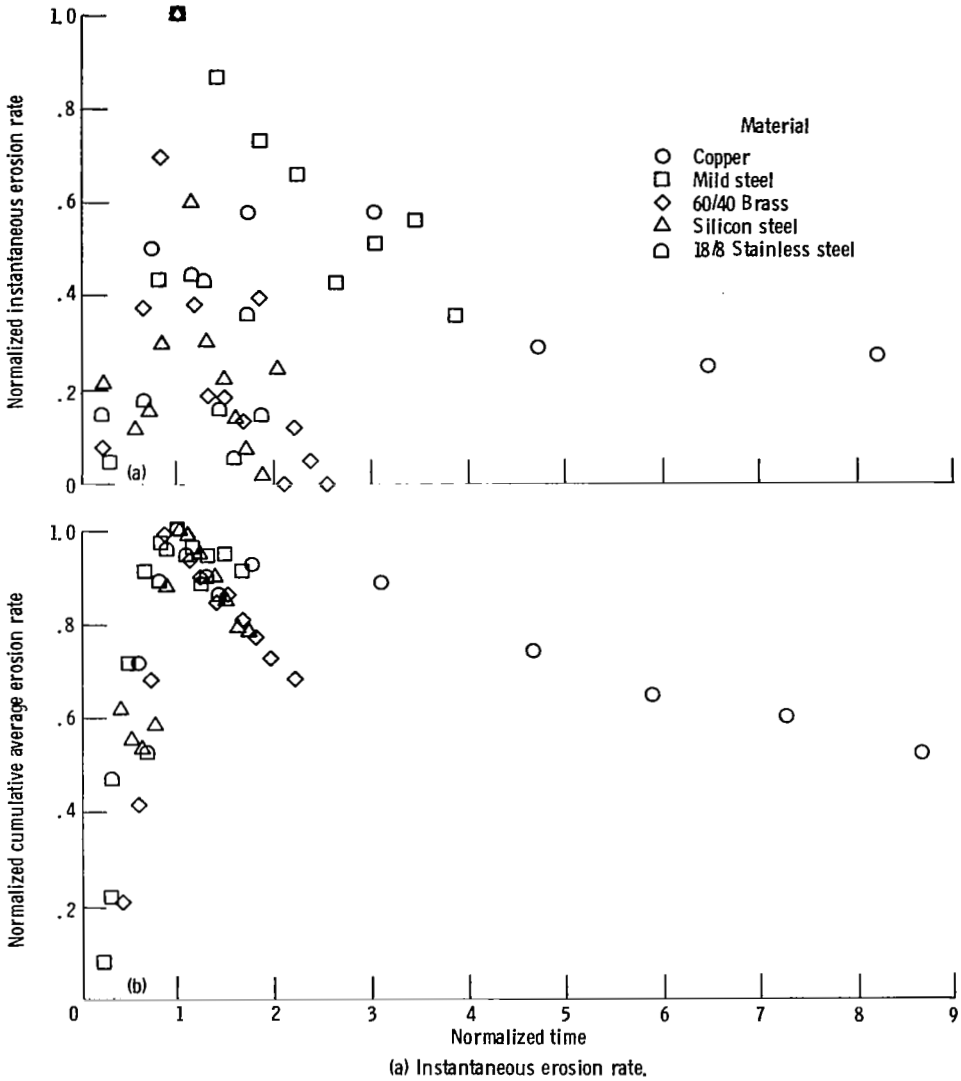

(a) Instantaneous erosion rate.

(b) Cumulative average erosion rate.

Figure 19. - Normalized erosion rate versus normalized time for various materials tested in liquid impingement. (Data from ref. 26.)

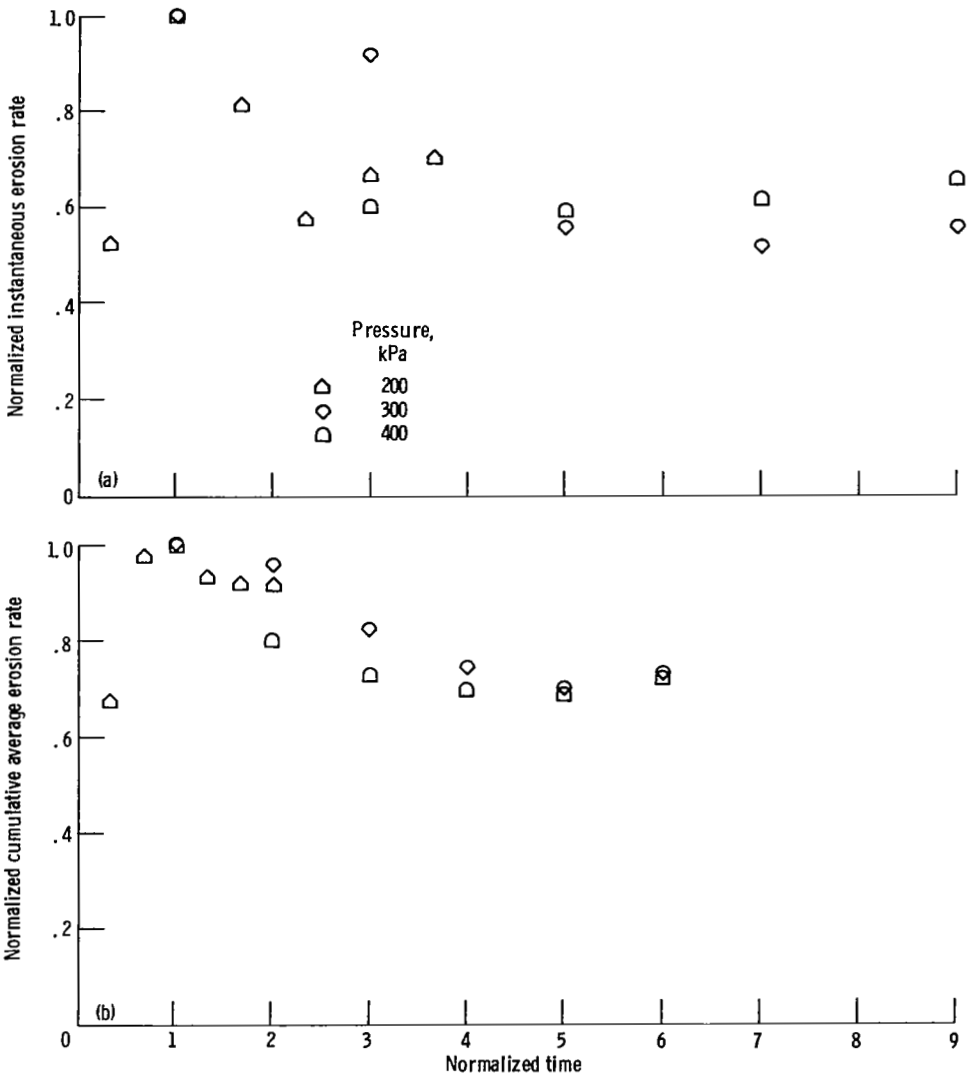

(a) Instantaneous erosion rate.

(b) Cumulative average erosion rate.

Figure 20. - Normalized erosion rate versus normalized time for L-605 alloy tested in magnetostriction apparatus at 427° C in liquid sodium - 1-hour time intervals.

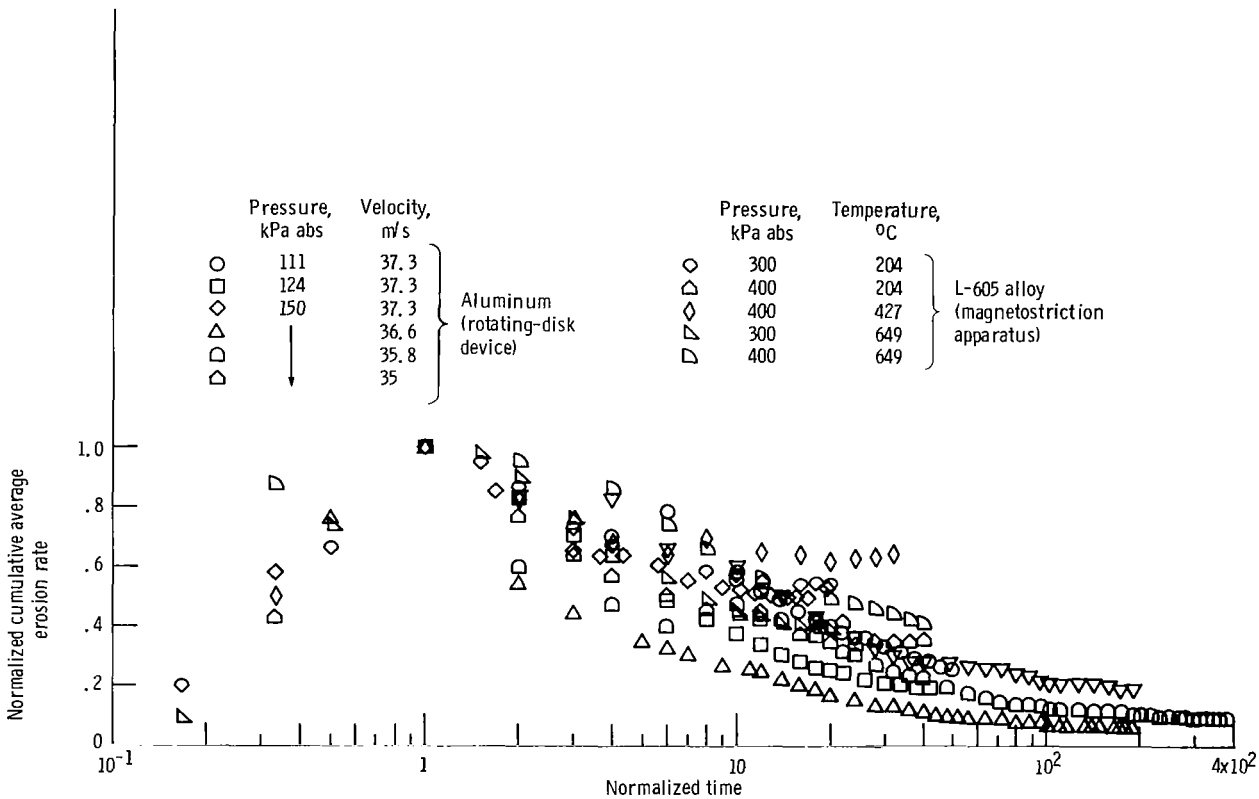

Figure 21. - Normalized cumulative average erosion rate versus normalized time for long exposures.

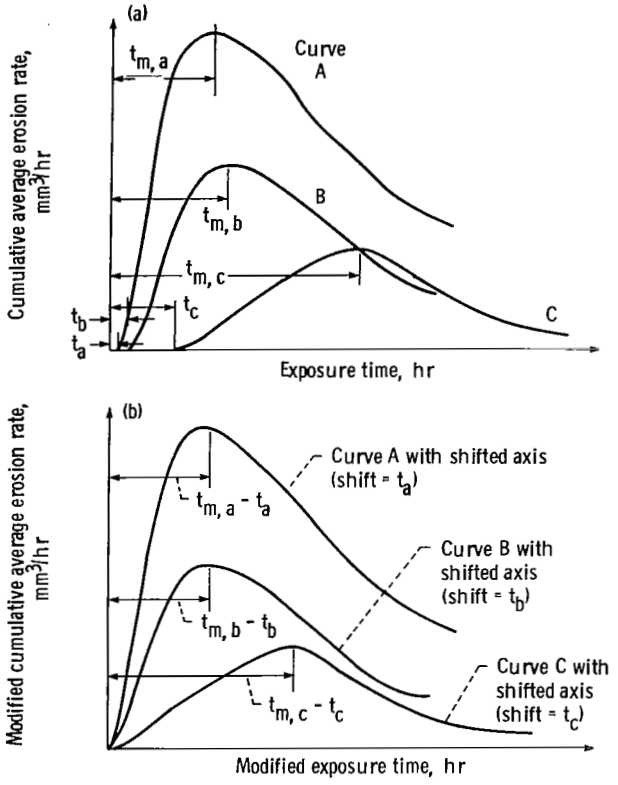

(a) Typical cumulative average erosion rate versus time curves.

(b) Modified cumulative average erosion rate versus modified time curves.

Figure 22. - Effect of incubation period correction, where t_a, t_b, and t_c denote the incubation periods of curves A, B, and C, respectively, and $t_{m,a}$, $t_{m,b}$, and $t_{m,c}$ denote times to attain maximum rates of erosion of curves A, B, and C, respectively.

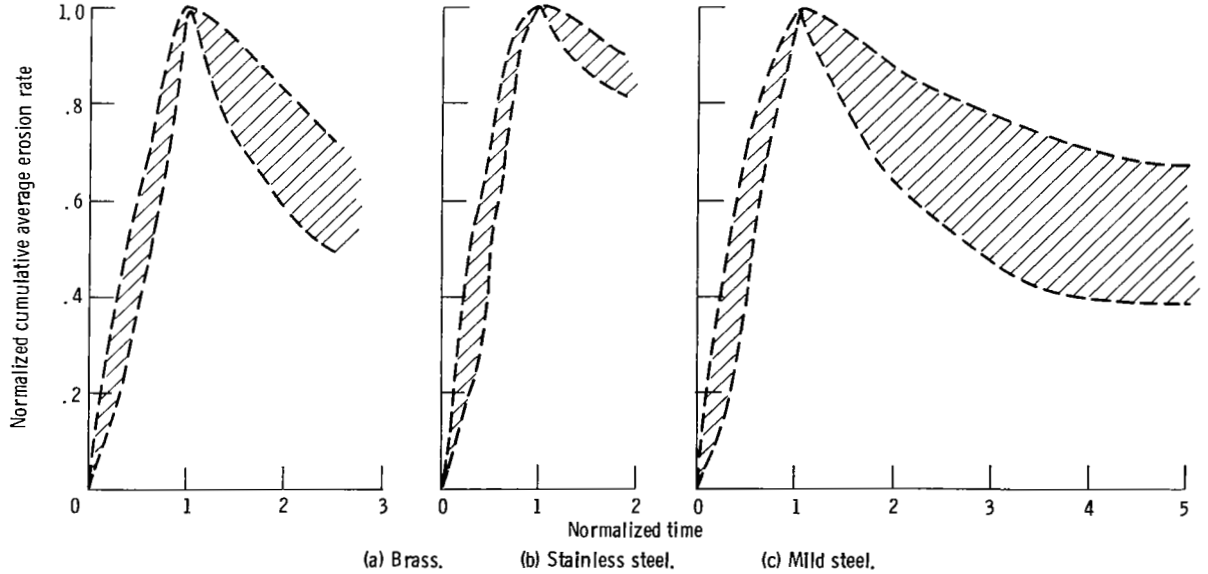

(a) Brass. (b) Stainless steel. (c) Mild steel.

Figure 23. - Summary plots for brass, stainless steel, and mild steel.